Fundamentals and Applications of Electrowetting: A Critical Review

Ya-Pu Zhao* and Ying Wang

State Key Laboratory of Nonlinear Mechanics, Institute of Mechanics Chinese Academy of Sciences, Beijing 100190, China

Abstract: We have witnessed rapid and exciting development in electrowetting (EW) or electrowetting-on-dielectric (EWOD) since 1990s. Owing to its great advantages such as easy operation, sensitive response and electrical reversibility, EW has found many applications in various fields, especially in micro- and nano-fluidics, electronic display, etc. The aim of this review is to inspire new investigations on EW, not only in theory and numerical simulation, but also in experiments, and spur further research on EW for more practical applications. A comprehensive review is presented on the EW research progress, and experiments, theoretical modeling and numerical simulations are covered. After a brief look at the development history, some latest experimental and simulation methods, such as Lattice Boltzmann method, phase-field method and molecular dynamics (MD), are introduced. Some representative practical applications are then presented. Unresolved issues and prospects on EW as the final part of this review are expected to attract more attention and inspire more in-depth studies in this fascinating area.

Keywords: Electrowetting (EW), electrowetting-on-dielectric (EWOD), Lippmann-Young (L-Y) equation, curvature effect, elasto-electro-capillarity (EEC), Lattice Boltzmann method (LBM), phase-field model, molecular dynamics (MD) simulations, coffee stain ring, electronic display, liquid lens, Micro Total Analysis Systems (μ-TAS), cell-based digital microfluidics

1 Motivation

Electrowetting (EW) or electrowetting-on-dielectric (EWOD) is an indispensable and versatile means for droplet manipulation. It was developed from elecrtrocapillarity [1, 2] by Lippmann in 1875 [3] in his PhD thesis, but did not attract much attention until the 1990s, when EWOD was proposed [4, 5]. Ever since then, EWOD

**Corresponding author*: yzhao@imech.ac.cn

DOI: 10.7569/RAA.2013.097304

has been developing fast, and has been put into applications in various fields, such as 'lab-on-a-chip' devices [6, 7], adjustable lenses [8], and electronic display technology [9]. Most current studies and applications concentrate on EWOD rather than EW, so the concepts of EWOD and EW are often without strict distinction and EWOD is often called as EW for short, except in special cases.

Owing to technological and consumer demands, miniaturization is the inevitable trend for microelectromechanical systems (MEMS) and nanoelectromechanical systems (NEMS). With decreasing system size, some physical and mechanical properties would become much different from macro-systems because of tremendous increase in the surface-to-volume ratios. This is one of the greatest challenges for the development of MEMS and NEMS, and thus for EW which is one of the useful methods used in the digital systems. Therefore, we review classical and latest fundamentals and applications of EW in this work, hoping to help better understanding of the EW phenomenon and promote further development in both fundamental studies and applications. For lack of space, we have concentrated on experimental and simulation methods, together with some of the modern applications.

A brief introduction to the development of EW is presented in section 2. Then simulation methods including Lattice Boltzmann method (LBM), phase-field method and molecular kinetic theory (MKT) are introduced, and how molecular dynamics (MD) simulations are used in EW are discussed in section 3. Experimental methods and some experiments in EW are discussed in section 4. Modern EW applications like display technology, liquid lenses, optic communication, micro total analysis systems (μ-TAS) and cell-based digital microfluidics are presented in section 5. Unresolved issues and prospects are given in section 6, followed by summary in section 7.

2 Brief Introduction to EW Development

A real surface can be either hydrophilic or hydrophobic, see Figure 1. The three interfacial tensions operate together at the triple line to maintain droplet equilibrium with a certain contact angle. When voltage is applied, the contact angle will

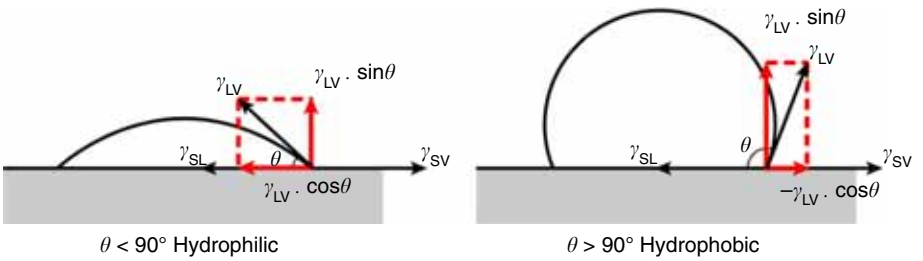

Figure 1 Droplet on a surface. The three interfacial tensions work together at the triple line to maintain tangent force equilibrium.

DOI: 10.7569/RAA.2013.097304

decrease to reach a new equilibrium value, i.e., voltage can enhance wettability of the surface. This phenomenon is called EW, which could be explained in the framework of surface and interface physical mechanics [10].

2.1 Brief History of EW and EWOD

In 1875, Lippmann [3] discovered that the capillary climb of mercury altered when a voltage was applied between the mercury and the electrolyte solution. This phenomenon is called electrocapillarity. Lippmann thought it was the induced residual charge that altered the solid-liquid interfacial tension γ_{SL}, and gave the equations:

$$\sigma_e = -\frac{\partial \gamma_{SL}}{\partial V}, \tag{1}$$

$$c = \frac{\partial \sigma_e}{\partial V}, \tag{2}$$

where σ_e is the surface charge density, V is the value of the applied voltage, c is the capacitance per unit area. The electrocapillarity phenomenon and the Lippmann equations are the basis of current EW. In the following centuries, this phenomenon was steadily studied [1, 2], from electrocapillarity to EW. However, electrolytic decomposition occurred when the applied voltage was increased to a few hundred millivolts [11] in early studies on EW, and thus it was hard to use EW for applications. This problem was solved by placing a thin dielectric film on the substrate to separate it from the liquid droplet instead of direct contact [4, 5]. The applied voltage can hence be increased to hundreds of volts. This form of EW is called EWOD. Berge [4, 5] carried out such experiments in the 1990s, including the application in liquid lenses, and gave the EWOD equation by combining Lippmann equations with the Young equation:

$$\cos\theta(V) = \cos\theta_0 + \frac{\varepsilon V^2}{2\gamma_{LV} d}, \tag{3}$$

where $\theta(V)$ is the contact angle under a certain voltage, θ_0 is the contact angle without applied voltage, ε is the dielectric constant, d is the thickness of the dielectric film. The last term of Eq. (3) is called the EW number:

$$E_W = \frac{\varepsilon V^2}{2\gamma_{LV} d}, \tag{4}$$

it represents the ratio of the electrostatic energy to the liquid-vapor interfacial energy [12]. Equation (3) has been found to be in good accord with the experimental results under low voltages, and is the fundamental equation of EWOD.

DOI: 10.7569/RAA.2013.097304

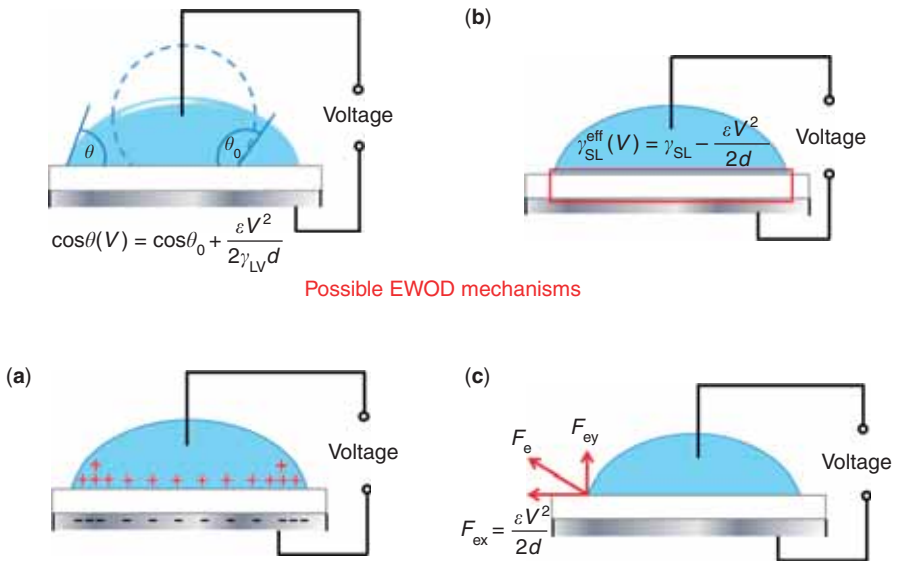

Figure 2 Upper left is the schematic of EWOD, and (a), (b), (c) are three main interpretations to EWOD mechanism. (a) Repulsion of the like-charges at the triple line: the repulsion leads to contact line moving and droplet spreading. (b) Effective capacitance: the dielectric film is taken as part of the solid-liquid interface and works as a capacitor. The effective solid-liquid interfacial tension changes when voltage is induced, i.e., $\gamma_{SL}^{eff}(V)=\gamma_{SL}-\frac{\varepsilon V^2}{2d}$. (c) Electromechanics: the Maxwell stress tensor or the electrostatic force "drags" the droplet to spread out.

The Lippmann-Young (L-Y) equation Eq. (3) can be derived from different approaches based on different mechanisms. Three approaches that are widely accepted are the thermodynamic approach, the energy minimization approach, and the electromechanical approach. More details can be found in [11] and [12]. The mechanism of EW is still debatable. Effective capacitance and electromechanics are the two main interpretations, see Figure 2. While in effective capacitance the dielectric film is taken as part of the solid-liquid interface to work as a capacitor and almost all of the electric energy is stored in it [11], and in electromechanics EWOD is considered as an electromechanical phenomenon [13], we think they are related. From the viewpoint of physical mechanics, the reduction of the contact angle may result from the repulsion of like-charges at the triple line.

The type of wetting (total or partial) when a liquid droplet is deposited on a substrate is determined by the spreading parameter S_p, which is defined as $S_p=\gamma_{SV}-(\gamma_{SL}+\gamma_{LV})$ without applied voltage [12]. Actually, the spreading parameter S_p is the difference between work of adhesion ($W_{\text{solid-liquid}}=\gamma_{LV}+\gamma_{SV}-\gamma_{SL}$) for solid-liquid interface and work of cohesion ($W_{\text{liquid-cohesion}}=2\gamma_{LV}$) for the liquid [10]. If $S_p>0$, the liquid completely wets the substrate; if $S_p<0$, the liquid forms a

DOI: 10.7569/RAA.2013.097304

droplet with a certain contact angle θ. In the case of EW, electric energy contributes to the spreading parameter [10]:

$$S_{\mathrm{p}} = \gamma_{\mathrm{SV}} - \left(\gamma_{\mathrm{SL}} + \gamma_{\mathrm{LV}}\right) + \frac{\varepsilon V^2}{2d}. \tag{5}$$

For EW at nanoscale, line tension and disjoining pressure should also be considered and the spreading parameter is [10]:

$$S_{\mathrm{p}} = \gamma_{\mathrm{SV}} - \left(\gamma_{\mathrm{SL}} + \gamma_{\mathrm{LV}}\right) + \sum_i |\boldsymbol{E}| \times |\boldsymbol{\mu}_i| \times L\left(\frac{|\boldsymbol{E}| \times |\boldsymbol{\mu}_i|}{k_{\mathrm{B}}T}\right) - \frac{\tau}{R} + \frac{A}{12\pi h^2}, \tag{6}$$

where $|\cdot|$ is the absolute value of a physical quantity, $\boldsymbol{E}$ the electric field vector, $\boldsymbol{\mu}_i$ the electric dipole moment, k_{B} the Boltzmann constant, T the absolute temperature, $L(x) = \coth(3x) - 1/(3x)$ the Langevin function, τ the line tension, A the Hamaker constant, R the radius of curvature at the contact line, and h the film thickness.

Ever since the 1990s, EWOD has entered into a period of rapid development. Applications that have been achieved or that are possible are flourishing in various fields. Liquid microlens [14–18] is a typical example of EWOD application, owing to the advantage of adjustable focal length that can be controlled by EWOD. It represents high quality, speed and reversibility. EWOD can also be used in electronic display technology [19], such as electronic paper (e-paper) [20–22]. The concept of rolltop which is a portable laptop with folding and unfolding substrate was once proposed on the Internet, and EWOD can be a promising means to achieve its application. Besides, EWOD is widely used in biomedical [23–25] and chemical [26–28] devices due to rapid and repeatable droplet manipulation and transportation ranging from nanoliters to microliters in volume [29]. Potential applications such as sample collection and preparation, DNA analysis and repair, protein recognition, and cell sorting [12] are also discussed.

Motivated by the needs of application, theoretical and experimental models for extended L-Y equations are developed. Contact angle is found to saturate around 30° to 80° under high voltages [4, 11, 30, 31], which could not be explained by the L-Y equation. Many studies have been carried out trying to explore EW under high voltage [32–37]. The L-Y equation is based on ideal assumptions, such as the surface is planar, smooth and isotropic, the liquid droplet is a perfect conductor and is deposited symmetrically on the substrate. However, real surfaces are always rough and curved, sometimes anisotropic, and the droplet can hardly be symmetrically deposited. Considering real conditions, a number of studies were conducted and extended L-Y equations were put forward, taking into consideration the surface roughness [38–41] and curvature [42]. Contact angle hysteresis is an accompanying phenomenon that always affects EWOD. The effects on the minimum actuation voltage and, therefore, on the droplet actuation were studied [7, 43–46]. Marangoni convection or temperature-induced effect should also be

DOI: 10.7569/RAA.2013.097304

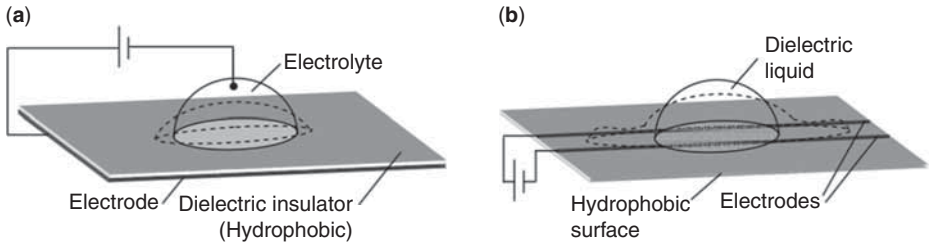

Figure 3 Schematics of Classical and Spontaneous electrowetting (EW) configurations [53]. (a) Classical EW configuration: a conducting droplet is deposited on electrode coated with a dielectric film. (b) Spontaneous EW configuration: a dielectric droplet is placed on a parallel line electrode.

considered, because the introduction of voltage may cause uneven heat distribution in the droplet and at the liquid-vapor interface [47, 48]. Since the L-Y equation was derived from and is applicable for EW in macroscopic systems, it neglects microscopic effects such as the line tension. Besides, the assumptions in the derivation may not be valid due to scale effect in that nanodroplet with size well below the Debye screening length will act differently from macroscopic droplets. Therefore, study on micro- and nano- EW is important [49–52]. Besides classical EWOD, variants such as spontaneous EW [53–55] are also studied. While a conducting droplet is placed on a dielectric film coated planar electrode in classical EWOD configuration, spontaneous EW adopts a parallel line electrode configuration, see Figure 3.

More details can be found in other reviews [11, 12, 56]. Different from these reviews, this article has mainly concentrated on experimental and simulation methods with relevant EW experiments and simulations, as well as some of the modern applications.

2.2 *From Elasto-capillarity to Electro-elasto-capillarity*

The previously mentioned EW works on a stable substrate. However, in the application field, the substrate is usually flexible and can be influenced by the liquid droplet sitting on it. Elasto-capillarity and electro-elasto-capillarity are kinds of wetting and EW, which take place on unstable substrates [57]. In 2004, Bico, *et al.* published their paper [58], reporting the mechanism of a common phenomenon—coalescence of wet hair. Hair (Figure 4a), a standard elastic fiber, could be bent by the surface tension of liquid, which is named as elasto-capillarity (EC). The length of the bent part of hair L_{dry} is determined by the following equation

$$L_{\mathrm{dry}}^4 = \frac{9}{2} d_{\mathrm{h}}{}^2 L_{\mathrm{EC}}^2 , \tag{7}$$

where d_{h} is the separation distance between hairs, L_{EC} is the elastocapillary length

DOI: 10.7569/RAA.2013.097304

$$L_{EC} = \sqrt{\frac{B}{\gamma_{LV}}}, \tag{8}$$

where B is the bending stiffness of hair. Considering that droplet always contacts the substrate with a certain contact angle larger than 0, L_{EC} can be modified as [10]

$$L_{EC} = \sqrt{\frac{B}{\gamma_{LV}\left(1+\cos\theta\right)}}. \tag{9}$$

Another example in nature also reveals the same mechanism. The spiders also utilize this phenomenon. It is found that the spider threads that run circumferentially around spider webs are typically coated with a viscous fluid [59, 60]. This fluid forms a series of fluid droplets, inside which the thread wraps into a series of coils (Figure 4f). When the prey strikes the web, the coil unravels within the drop, and the associated viscous damping prevents the prey from being ejected.

In 2007, Py *et al.* investigated the interaction of liquid and poly (dimethylsiloxane) (PDMS) thin film [61]. They found that under the actuation of surface tension, PDMS thin film could wrap the droplet spontaneously (Figure 4b and Figure 4c). In their

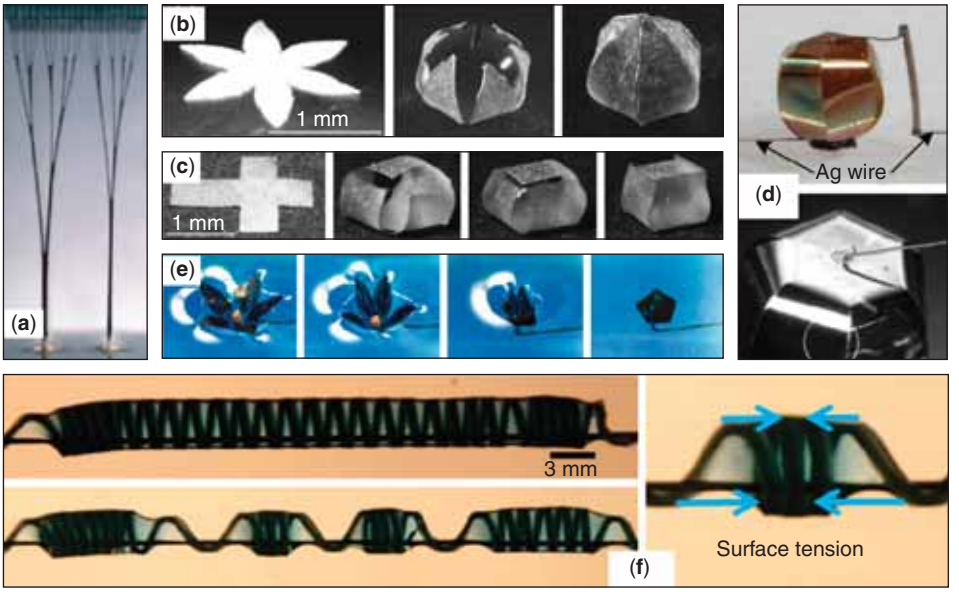

Figure 4 Experiments on elasto-capillarity. (a) Wet hair is bent by the surface tension of liquid [58]; (b) Capillary origami, a spontaneous wrapping of liquid droplet by PDMS film [61]; (c) A droplet is wrapped in the shape of box [61]; (d) Spherical solar cells self-assembled from flower-shaped flat Si leaflets [62]; (e) Artificial flower is folded when sunk into water [60]. (f) Spider threads wrap into coils by the action of surface tension [59, 60].

DOI: 10.7569/RAA.2013.097304

experiment, a slice of PDMS thin film was placed on the surface of a superhydrophobic surface, in order that the film would not stick to the substrate. Then they placed a droplet of water, whose size was larger than the characteristic length L_{EC}, and the wrapping spontaneously occurred. They tried different shapes of PDMS film to wrap the droplet and named it as "Capillary Origami".

The same capillary origami phenomenon does not happen to only PDMS thin film. In 2009 Guo *et al.* studied wrapping of a droplet by single-crystalline silicon [62]. They also applied EC to the field of photovoltaic power devices and fabricated the flower-shaped Si leaflet to build spherical solar cells (Figure 4d). Jamin *et al.* utilized a drop of magnetic fluid and studied the quasistatic and dynamical behaviors of such a magnetic capillary origami [63]. They observed an overturning instability that the origami underwent at a critical magnetic field. This instability resulted from an interaction between magnetic and gravitational energies. Van Honschoten and coworkers also fabricated a three-dimensional (3D) microstructure which would be folded into the shape of a box in the scale of 50 μm [64].

In nanoscale, Patra *et al.* carried out MD simulations to predict that nanodroplet could be wrapped by graphene thin film [65]. In this work, water nanodroplet activated and guided the folding of two graphene flakes. They demonstrated that nanodroplets can induce rapid bending, folding, sliding, rolling and zipping of the planar nanostructures, which can lead to assembly of nanoscale structures.

In the former cases, droplet is wrapped inside the film, however, surface tension will still work when liquid is outside the film. In 2009, work of Jung *et al.* showed that when submerging an artificial flower into water, the flower would be folded [60]. They also fabricated a microstructure, whose size was approximately 50 μm, and it sank into water. They found that the structure can be assembled in 3 dimensions (Figure 4e).

EC under droplet impact is also capable of 3D assembly of structures. In 2011, Antkowiak *et al.* reported that using droplet impact and EC, instant fabrication and selection of folded structure could be realized [66]. They compared experimental and simulation results of a droplet impact near the end of a strip and found that the location of impact point is important to determine whether the strip will wrap the drop or not (Figure 5). When the impact point is near the end, the strip will encapsulate the droplet very fast; however, if the impact point is far away from the end, the strip will not encapsulate the droplet because of its own gravity.

Though EC is a practical method for self-assembly of micro- and nanostructures, it is not a controllable procedure, after all. Yuan and Zhao introduced electric field into the wrapped water nanodroplet in MD simulations [52]. They found that under the application of electric field, graphene film will be pushed open and the nanodroplet can be released.

In experimental researches, Pineirua *et al.* found a way to control capillary origami with electric field [67]. They found that it is possible to open the closed origami structure if a sufficiently strong electric field is imposed between the droplet and the counter electrode.

DOI: 10.7569/RAA.2013.097304

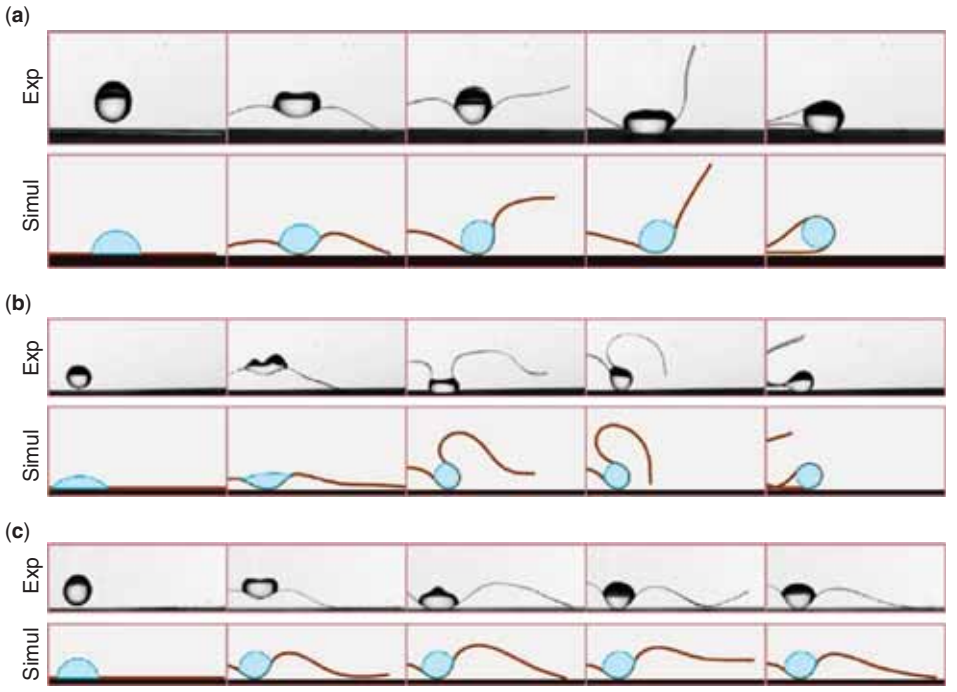

Figure 5 The impact induced instant fabrication and selection of folded structures [66]. (a) 'Rigid' encapsulation observed when $x/l_{eg} \leq 1$; (b) 'Floppy' encapsulation: for larger value of x/l_{eg}, the free end of the film folds so as to mitigate the influence of gravity; (c) when the drop is deposited too far from the end of the strip, capillary forces cannot overcome the weight of the strip and the drop remains unencapsulated.

In 2012, Wang *et al.* applied direct current (DC) voltage and alternating current (AC) voltage to the wrapped droplet [68] and discovered that electric field is not only able to unwrap the droplet, but also provokes the droplet to vibrate, and Zhao named it as electro-elasto-capillarity (EEC).

In their experiments, a tiny salty droplet is located on the surface of a flexible thin (70 μm thick) PDMS film. The film is placed on a ZnO superhydrophobic surface. When electric field is applied, the PDMS film tends to unwrap the drop because of the combined effect of Coulombic force, surface tension and elastic force (Figure 6a). When the voltage reaches a critical value, about 650 V in this experiment, the film is pulled into the substrate and releases the droplet completely (Figure 5).

When an AC voltage is applied, the droplet begins to vibrate, just like it is tap dancing, so they also called it "Tap dance of water droplet". They discovered that the vibration frequency of film is twice the AC frequency (Figure 6b).

They also swept the input frequency and found three resonance peaks (Figure 6c). The first peak appears when the input frequency is around 40 Hz.

DOI: 10.7569/RAA.2013.097304

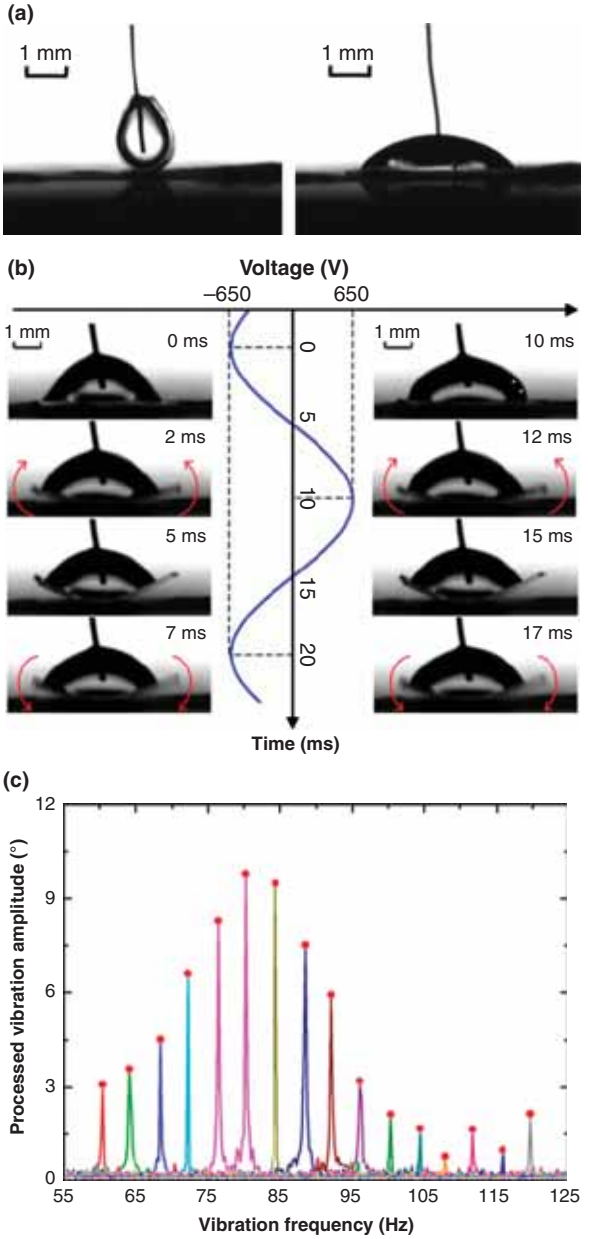

Figure 6 Electro-Elasto-Capillarity. (a) Thin film wraps the droplet when there is no voltage and the film unwraps the droplet when the voltage reaches a certain value; (b) Tap dance of water droplet: under the actuation of AC voltage, the film and the droplet start to vibrate; (c) A resonance peak is found when the frequency of the applied voltage is 40 Hz and the vibration frequency is about 80 Hz [68].

DOI: 10.7569/RAA.2013.097304

This frequency is near the free vibration frequency of a 2 mm water droplet, according to Lord Rayleigh.

2.3 EW on Curved Surfaces

The surge of interest in the EW on curved surfaces which is still going on today began in 1990s. The situation is that EW on curved surfaces has found wide applications, nevertheless, the fundamental equation for EW on curved surfaces has been lacking until 2011. The L-Y equation, describing the relation between the contact angle and the applied voltage on planar surfaces, should be modified to take the surface curvature effect into account.

Wang and Zhao [42] were the first to systematically study the surface curvature effect from theoretical aspect. Here on spherical surfaces, the contact angle θ is defined as the angle between the solid-liquid surface tangent and the liquid-vapor surface tangent, as illustrated in Figure 7a. By using the principle of energy minimization, an extended L-Y equation on spherical surfaces (Figure 7a) was proposed:

$$\cos\theta(V) = \cos\theta_0 + \frac{\varepsilon V^2}{2\gamma_{LV} d} \cdot \frac{1}{1 \pm a}, \tag{10}$$

where $a = d / R$ is the ratio of the thickness of dielectric film to the radius of the spherical substrate. Equation (10) means that for a convex surface

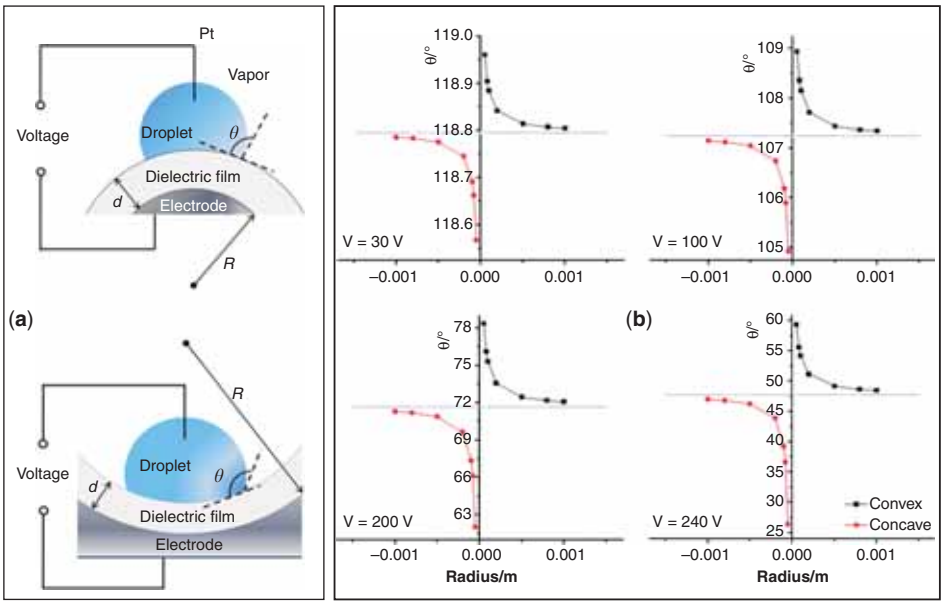

Figure 7 (a) Schematic of EWOD on curved (convex and concave) surfaces; (b) Contact angle θ versus the radius of the spherical substrate under different applied voltages V [42].

DOI: 10.7569/RAA.2013.097304

$$\cos\theta(V) = \cos\theta_0 + \frac{\varepsilon V^2}{2\gamma_{LV} d} \cdot \frac{1}{1+\alpha}, \tag{10a}$$

and for a concave surface

$$\cos\theta(V) = \cos\theta_0 + \frac{\varepsilon V^2}{2\gamma_{LV} d} \cdot \frac{1}{1-\alpha}. \tag{10b}$$

The last term in equation (10) is a dimensionless number, which is called the curvature-modified EW number:

$$E_W^* = \frac{\varepsilon V^2}{2\gamma_{LV} d} \cdot \frac{1}{1\pm\alpha}. \tag{11}$$

It represents the ratio of electrostatic energy to interfacial energy. So the EW equation on spherical surfaces can also be expressed as:

$$\cos\theta(V) = \cos\theta_0 + E_W^*. \tag{12}$$

As the capacitance of a spherical capacitor per unit area is $c = \varepsilon / \left[d(1\pm\alpha) \right]$, Eq. (10) can be simplified as

$$\cos\theta(V) = \cos\theta_0 + \frac{1}{2} \cdot \frac{cV^2}{\gamma_{LV}}, \tag{13}$$

where c is the capacitance per unit area. Although it is derived from the specific case of a spherical surface, it is actually always applicable for EW on surfaces with various curvatures. This means that for EW on curved surfaces under low voltage, once the capacitance per unit area is known, the contact angle can be predicted. The L-Y equation can be seen as a degenerate equation considering the surface curvature effect by substituting the capacitance of a parallel-plate capacitor per unit area $c = \varepsilon / d$ into Eq. (13). However, it should be noted that since the mechanism of EW is still debatable, the extended EW equation is not simply a problem of capacitor, though it can be simplified as the form of capacitance.

According to the theory, with decreasing system size, the surface curvature effect becomes even more significant, see Figure 7b. In present experimental conditions, α (the ratio of d to R) is small, making the modified EW number close to 1. In this case, the variation of the contact angle on curved surfaces is close to that on planar ones, and surface curvature effect is not that obvious. This prediction is in good accord with experimental results. Kim and Steckl [69] compared EWOD on rolled-paper substrate with different materials in order to explore the feasibility of using paper as a cheap and flexible substrate for e-paper, electronic display and other EW devices. Fan and co-workers [19] studied "droplet-on-a-wristband" which can be used in flexible electronic devices. They conducted experiments on curved surfaces with curvatures 0, 0.02, 0.04 and 0.06 mm^{-1}, and explored the required driving voltages at the center point. Wheeler's group [70] built all-terrain

DOI: 10.7569/RAA.2013.097304

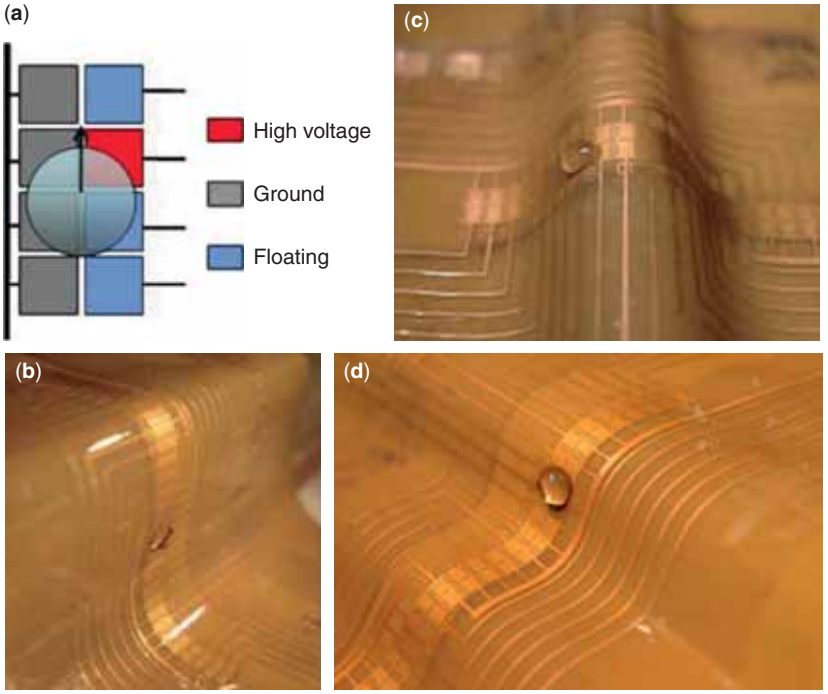

Figure 8 All-terrain droplet actuation (ATDA) manipulation [70]. (a) Actuation scheme. (b) Droplet moving up a 15 mm high wall. (c) Droplet moving up a "bridge". (d) Droplet moving down a staircase.

droplet actuation (ATDA) model and conducted relevant experiments (Figure 8), in which substrate curvature was variable. In the above studies, experiments are at the macroscopic level, and it is found that the surface curvature effect is not that noticeable.

However, when R becomes very small, i.e., micro- and nano-scale EWOD, such as EW in carbon nanotubes (CNTs) and on graphene substrate, the surface curvature effect will become significant and cannot be neglected. Chen et al. [71] studied EW in CNTs by molecular dynamics (MD) simulations. They considered the influence of the surface curvature and adopted Lippmann's model of EW for a cylindrical capacitor. Nevertheless, there are only a few experiments on and below microscale in the published work, so further investigation is needed.

Since a curved surface can be either convex or concave, the change in the contact angle is different. While the contact angle on convex surfaces decreases compared to that on planar ones, it increases on concave surfaces. This means concave surfaces can enhance wettability better than convex surfaces under the same voltage, which can guide the applications.

DOI: 10.7569/RAA.2013.097304

At the end of this part, considering the line tension which works on and below microscale, we present a uniform expression for EW on various geometrical surfaces [42]:

$$\cos\theta(V) = \cos\theta_{\mathrm{Y}} - \frac{\tau\chi}{\gamma_{\mathrm{LV}}} + \frac{1}{2}\cdot\frac{cV^2}{\gamma_{\mathrm{LV}}}, \tag{14}$$

where θ_{Y} is the Young contact angle, τ the line tension, χ the geodesic curvature [72], and c is the capacitance per unit area.

3 Simulation Methods and Simulations in EW

3.1 Lattice Boltzmann Method (LBM)

Lattice Boltzmann method (LBM) is a numerical scheme based on the kinetics of mesoscopic particles. It is suitable for simulating fluid flows involving complex boundaries and interfacial dynamics [73]. LBM has special advantages because of the fact that it is a combination of macroscopic method and microscopic method. And it is computationally efficient and available for parallel computing. In LBM, the Navier-Stokes equations are solved through the evolution of a set of distribution functions $f_i(r,t)$. The collisions and displacements of the mesoscopic particles are controlled by the following LB equation:

$$f_i\left(r + c_i\Delta t, t + \Delta t\right) - f_i\left(r,t\right) = -\frac{1}{\tau}\left[f_i\left(r,t\right) - f_i^{\mathrm{eq}}\left(r,t\right)\right], \tag{15}$$

where Δt is the time step, c_i the component of velocity tensor $\boldsymbol{c}$, τ the relaxation parameter and $f_i^{\mathrm{eq}}(r,t)$ the equilibrium distribution function. The macroscopic quantities are expressed by the moments of $f_i(r,t)$. For example, the density ρ and macroscopic velocity $\boldsymbol{u}$ are defined by

$$\rho = \sum_i f_i, \quad \rho\mathrm{u} = \sum_i f_i \mathrm{c}_i. \tag{16}$$

LBM has been extended to model EW mainly through two versions of LBM (Table 1): the Shan-Chen multiphase model [74, 75] and the free energy-based approach [76–78].

3.1.1 Shan-Chen Multiphase Model

In this version, the interactions among particles are modeled by considering the microscopic interactions to modify the surface-tension–related collision operator [74, 75]. The interaction potential is defined by

$$V\left(\mathrm{x},\mathrm{x}'\right) = G_{kk'}\left(\mathrm{x},\mathrm{x}'\right)\varphi^k\left(\mathrm{x}\right)\varphi^{k'}\left(\mathrm{x}'\right), \tag{17}$$

in which $G_{kk'}(\mathrm{x},\mathrm{x}')$ is a Green function and $\varphi^k(\mathrm{x})$ a function of density for the kth phase at $\mathbf{x}$ which takes the form $\varphi^k(\mathbf{x}) = \rho_0\exp\left(-\rho_0/\rho\right)$, where ρ_0 is a constant free parameter. The interface can be maintained automatically in this model.

DOI: 10.7569/RAA.2013.097304

Table 1 The main studies in the investigation of electrowetting through Lattice Boltzmann Method.

Year	Reported by	Title	Method
2009	Aminfar and Mohammadpourfard [86]	Lattice Boltzmann method for electrowetting modeling and simulation	Free energy-approach with D3Q15
2009	Li and Fang [79]	Lattice Boltzmann simulation of electrowetting	Shan-Chen multiphase model with D2Q9
2009	Clime *et al.* [82]	Numerical modeling of the splitting of magnetic droplets by multiphase lattice Boltzmann equation	Shan-Chen multiphase model with D2Q9
2010	Clime *et al.* [84]	Numerical modeling of electrowetting processes in digital microfluidic devices	Shan-Chen multiphase model with D3Q19
2012	Aminfar and Mohammadpourfard [87]	Droplets merging and stabilization by electrowetting: Lattice Boltzmann study	Free energy-approach with D3Q15
2012	Li and Fang [81]	Hysteresis and saturation of contact angle in electrowetting on a dielectric simulated by the Lattice Boltzmann method	Shan-Chen multiphase model with D2Q9
2012	Huang *et al.* [88]	A phase-field-based hybrid Lattice-Boltzmann finite-volume method and its application to simulate droplet motion under electrowetting control	Hybrid LBM–FVM numerical model

DOI: 10.7569/RAA.2013.097304

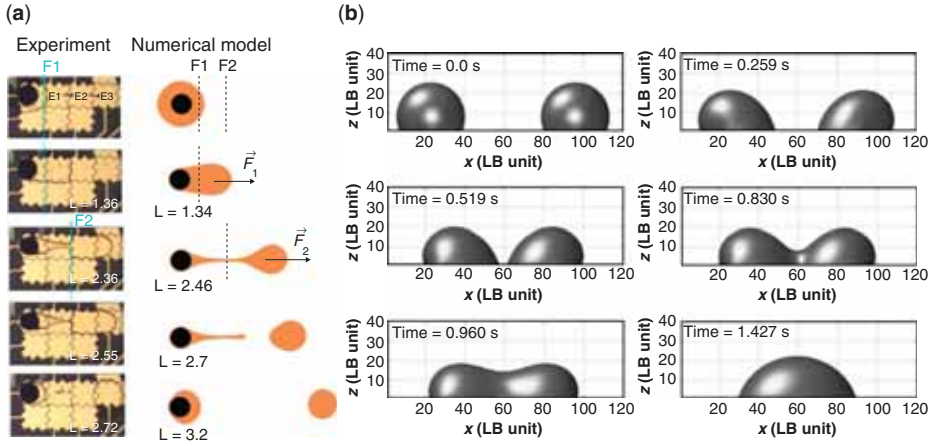

Figure 9 Droplet manipulation controlled by electrowetting through LBM. (a) Splitting of a magnetic droplet on three electrodes [82]. Left: splitting process by experiments. Right: splitting process by LBM. (b) Two droplets merging by electrowetting [87].

Li and Fang [79] used this model to simulate the EW of an electrolyte droplet by taking into account the electric force $\mathbf{F}_e$ applied to the substrate with D2Q9 LBM scheme [80]. They obtained the variation of the cosine of contact angle with respect to the applied voltage. The results are consistent with the L-Y equation under different strengths of fluid-fluid interactions and fluid-solid interactions. Recently, they observed the hysteresis and saturation of the contact angle in EW both on flat and rough surfaces through the same method [81]. And this effect was found to be more pronounced on rough surfaces. It was reported that wide grooves result in the contact angle saturation and narrow grooves induce hysteresis. In addition, they showed that the voltage can effectively control the electrolyte flow in a rough-wall channel.

The Shan-Chen multiphase model has been employed to realize the splitting of a 2D magnetic droplet in EWOD-based microfluidic devices by Clime *et al.* [82] with D2Q9 LBM scheme. The results showed good agreement with experiments as shown in Figure 9a. Then the 3D D3Q19 LBM scheme [83] was used to perform the basic operations involved in EWOD devices such as droplet transport, merging and splitting [84, 85].

3.1.2 Free Energy-based Approach

Unlike the Shan-Chen model which is based on the use of an interaction pseudopotential between different phases and is most suitable for isothermal multicomponent flows, the free-energy approach considers the energy minimization through thermodynamics to determine the equilibrium distribution. This approach was first introduced by Swift and coworkers [76, 77]. To overcome the lack of Galilean

DOI: 10.7569/RAA.2013.097304

invariance in the original version, this approach was further extended by Holdych *et al*. [78].

In 2009, Aminfar and Mohammadpourfard expanded this model to simulate EW [86]. In this approach, a free-energy functional is defined. In the case of EW, there are three components of energy: the electrostatic energy, the chemical free energy, and the mechanical free energy. Through energy minimization, the surface tensions were obtained, in which the electric contribution is dependent on the electric potential. Then the electric potential was calculated by solving the discretized Poisson-Boltzmann equation. They found that the potential distribution is exactly one-dimensional (1D) for a microdroplet. The 3D droplet spreading and motion due to EW were simulated which showed good agreement with experiment. In their recent work, this approach was further used to realize droplet merging in EW (Figure 9b) [87]. They also studied the droplet stabilization in the same article and concluded that an unstable droplet can be stabilized by applying a voltage.

Recently, Huang *et al.* proposed a hybrid method which integrates LBM for fluid flows and finite-volume method for interface dynamics to overcome the limitations of LBM in interface dynamics and keep the advantages of LBM for hydrodynamics [88]. They applied this new method to simulate the AC voltage controlled EW of droplets. Then the droplet motion controlled by EW was studied and the effect of the electric field on the droplet oscillation was investigated. They reported that the droplet oscillation amplitude varies approximately linearly with the change in contact angle under the maximum voltage. This work promises to provide valuable guidance for enhancing mixing controlled by EW.

3.2 Phase-field Method

The L-Y equation focuses on static cases, giving the apparent contact angle under a specific applied voltage. However, when voltage is induced, the contact angle decreases until reaching its stable value. This is a dynamic process during which the shape of the droplet is varying. Compared to static characterization, dynamic process includes more physical details, the study of which can provide a better understanding of EW. Besides, for many practical applications, dynamic properties are of great interest. Therefore, dynamic EW has attracted more and more attention, becoming a hot research area.

The study of the behavior of the liquid-vapor interface can be an approach for description of dynamic EW process. The Huh-Scriven paradox [10] predicts infinite stress and energy dissipation at the triple-phase contact line, by imposing continuum mechanics and no-slip boundary condition. Many studies have been carried out to solve the Huh-Scriven paradox, and several possible mechanisms have been proposed [89]. Diffuse interface is one of the solutions, by taking the interfaces between different phases with a small but finite thickness instead of sharp ones. The phase-field method, which is based on the diffuse interface model, can be a way to explore the details of the dynamic flow fields inside the droplet.

DOI: 10.7569/RAA.2013.097304

The phase-field method in an EW problem involves three physical models, i.e., the incompressible flow model, the phase-field or diffuse-interface model, and the model of droplet motion under electric field. The phase-field ϕ should be defined first so that $\phi = 1$ and $\phi = -1$ correspond to the liquid and vapor phases, respectively. Therefore, the details of the dynamic flow fields inside the droplet can be clarified by solving three equations with relevant boundary and initial conditions [90].

a. The incompressible flow equation:

$$-\nabla p' + \nabla \cdot \left(\eta(\phi) T(\boldsymbol{u})\right) + \boldsymbol{F}_{\mathrm{st}} + \boldsymbol{F}_{\mathrm{p}} + \boldsymbol{F}_{\mathrm{e}} = \boldsymbol{0}\,, \tag{18}$$

with boundary conditions:

$$\boldsymbol{u} \cdot \boldsymbol{n} = 0, \quad \text{in } S\,, \text{ (impenetrability)} \tag{19}$$

$$\beta \boldsymbol{u} \cdot \tau = -\eta(\phi)\left[\boldsymbol{n} \cdot T(\boldsymbol{u}) \cdot \boldsymbol{\tau}\right] + L\frac{\partial \phi}{\partial \tau}, \quad \text{in } S\,, \text{ (Navier boundary condition)} \tag{20}$$

and conditions on $\partial\Omega \setminus S$ which may vary with specific problems. For simplicity, conditions on $\partial\Omega \setminus S$ can be taken the same as those in S, where Ω is the domain occupied by the two phases (liquid and vapor), and S is the solid-liquid interface.

Here, p' is defined as $p' = p - \frac{\zeta}{2}\sigma^2$, where p is the pressure, ζ is a parameter far less than 1, σ is the amount of charge; $T(\boldsymbol{u}) = \frac{1}{2}\left[\nabla \boldsymbol{u} + (\nabla \boldsymbol{u})^{\mathrm{T}}\right]$, where $\boldsymbol{u}$ is the velocity; $\boldsymbol{n}$ is the unit normal vector, $\boldsymbol{\tau}$ is the unit tangent vector; $\eta(\phi)$ and β are viscosity coefficient parameters.

In Eq. (18),

$$\boldsymbol{F}_{\mathrm{st}} = \gamma_{\mathrm{lv}}\left[-\delta\Delta\phi + \frac{W'(\phi)}{\delta}\right]\nabla\phi\,, \tag{21}$$

$$\boldsymbol{F}_{\mathrm{p}} = -\left|\boldsymbol{E}\right|^2 \frac{\nabla\varepsilon(\phi)}{2}\,, \tag{22}$$

$$\boldsymbol{F}_{\mathrm{e}} = \rho \boldsymbol{E}\,, \tag{23}$$

are the surface tension, ponderomotive and electrostatic forces, respectively, where δ is a small positive parameter, $W'(\phi)$ is a bistable potential which is usually taken as $\left(1-\phi^2\right)^2$, $\varepsilon(\phi)$ is the dielectric constant, and $\boldsymbol{E}$ is the electric field.

b. The phase equation: the phase-field ϕ follows the Cahn-Hilliard equation:

$$\frac{\partial \phi}{\partial t} + \nabla \cdot (\phi \boldsymbol{v}) = -\nabla \cdot \boldsymbol{J}_{\phi}\,, \tag{24}$$

with boundary conditions:

$$\boldsymbol{J}_{\phi} = 0, \quad \text{in } S\,, \tag{25}$$

DOI: 10.7569/RAA.2013.097304

$$z\dot{\phi} = -L = -\left[\gamma'_{sf}(\phi) + \delta\frac{\partial\phi}{\partial n}\right], \quad \text{in } S, \tag{26}$$

$$\frac{\partial\phi}{\partial n} = 0, \quad \text{in } \partial\Omega \setminus S, \tag{27}$$

where $\boldsymbol{J}_\phi$ is the diffusion flux, and z is a phenomenological parameter. $\gamma_{sf}(\phi)$ is a smooth function to interpolate the values of the liquid-solid and vapor-solid interfaces when $\phi = \pm 1$.

c. Equation for electric charge density:

$$\frac{\partial\rho}{\partial t} + \nabla\cdot(\rho\boldsymbol{v}) = \nabla\cdot\left[K(\phi)\boldsymbol{E} + D(\phi)\nabla\rho\right] + q(s,t)\delta_{S_0}, \tag{28}$$

with boundary conditions:

$$\left[K(\phi)\boldsymbol{E} + D(\phi)\nabla\rho\right]\cdot\boldsymbol{n} = 0, \quad \text{at } \partial\Omega, \tag{29}$$

$$V = \overline{V}, \quad \text{at } \partial\Omega^*, \tag{30}$$

where $q(s,t)$ is the amount of charge at a specific point, S_0 is the region occupied by the electrode, Ω^* is a larger domain so that $\Omega \subset \Omega^*$ (with $\rho = 0$ at $\Omega^* \setminus \Omega$) and the voltage is applied at $\partial\Omega^*$. More details can be found in [90].

EW is a multi-field coupling problem, for which an analytical solution is difficult so numerical simulations are often used [88, 90]. However, since use of phase-field method for EW is still in its initial stage, further studies are needed.

In the phase-field method, it has no strict limit on the boundary condition, i.e., slip or no-slip boundary condition. Because of the diffuse interface, the Huh-Scriven paradox does not exist in this method. However, dynamic EW always involves contact line movement [56]. The moving contact line (MCL) problem in wetting has been studied for years. The two models that are widely accepted are hydrodynamic theory and molecular kinetic theory (MKT) [91]. The MCL problem will become more complicated if voltage is applied and thus needs further studies.

3.3 Molecular Dynamics (MD) Simulations

EW is a multiscale problem, which should be solved by multiscale methods (Figure 10). With the rapid development of nanofluidics, nanoscale EW has attracted more and more attention in recent years [92–94]. Within the framework of continuum theory, the whole system is described by macroscopic quantities and the intermolecular structures are ignored. The theory within the continuum assumptions is in good accord with the macroscopic EW experiments. But at nanoscale, the intermolecular forces or disjoining pressure should be considered, making the approximation underlying the continuum picture no longer valid. In addition, experiments at nanoscale are also difficult to perform. To overcome the limitations of experiments and continuum theory, MD simulations were employed

DOI: 10.7569/RAA.2013.097304

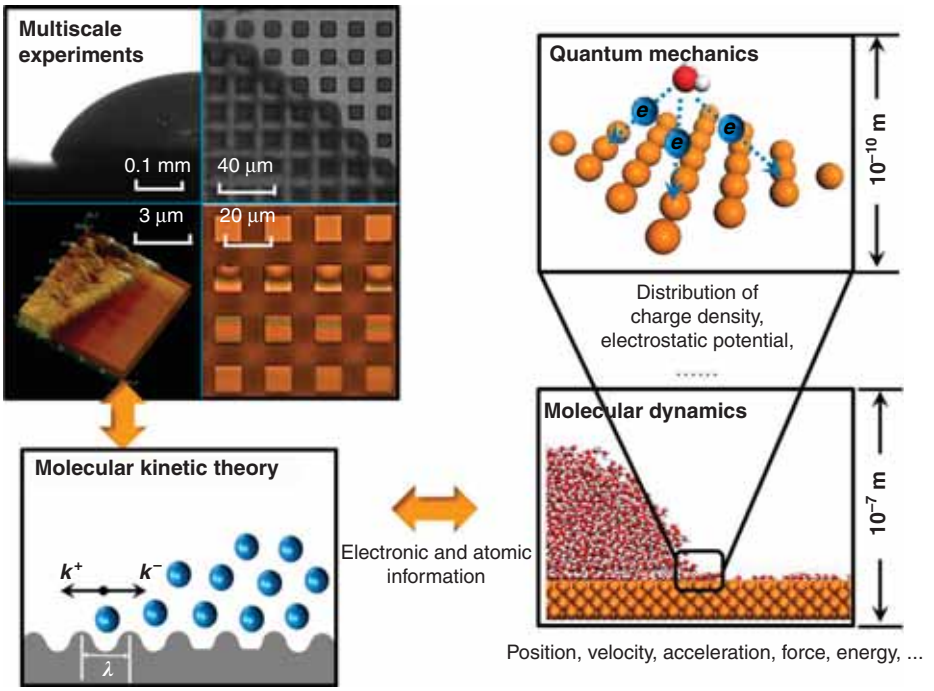

Figure 10 Multiscale methods for EW. At the electronic scale, quantum mechanics could be used to obtain the distribution of charge density and electrostatic potential (upper right). At the atomic scale, molecular dynamics (MD) could be used to obtain the position, velocity, acceleration of the spreading droplet, etc (lower right). Then the electronic and atomic information is transferred to the molecular kinetic theory (lower left). Combined with multiscale experiments (upper left), EW, which is a mutiscale problem, could be solved.

and MKT was developed recently. MD simulations can not only be used to capture the atomic details, but also to predict the phenomena at nanoscale.

Through MD simulations, new mechanisms [50, 52, 95–99] and new phenomena [71, 100–111] were found for EW at nanoscale, which spurred new applications. For example, Liu *et al.* found that the contact angle saturation in EW is caused by the molecules being pulled from the droplet and the saturation occurs if the peak electric force near the edge of the droplet exceeds the molecular binding force [98]. By applying an electric potential at a carbon nanotube, a notable driving force is produced for driving mercury to wet the inner core of the nanotube [71, 100, 104, 107] (Figure 11a). Ordered new structures can be formed on surfaces under external electric field as predicted by MD simulations [106, 111] (Figure 11b). MD simulations also showed that the electric-driven flows through nanochannels have potential applications for molecular water pump [102] (Figure 11c), particle

DOI: 10.7569/RAA.2013.097304

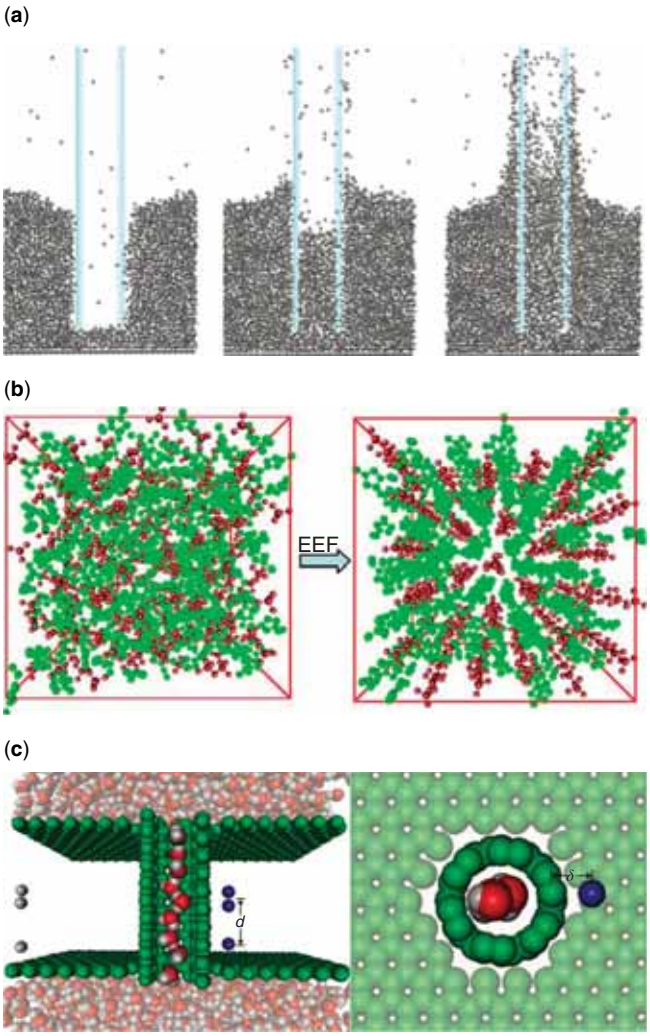

Figure 11 (a) Electrowetting of mercury in a (20, 20) carbon nanotube. Left: nonwetting meniscus outside the nanotube without applied electric field. Middle and right: 330 ps after application of 3.5 V and 4.0 V, respectively [100]. (b) Left: the state of ionic liquid without electric field. Right: ordered structure in the electric field of 1.14 V/Å [111]. (c) Molecular water pump via electric-driven flows through carbon nanotubes. Left: sideview of the main system. The blue spheres are positive charges, while the grey ones are negative charges. Right: topview of the same arrangement [102].

DOI: 10.7569/RAA.2013.097304

separation [101] and sensors [112]. In following discussions, we mainly review the basic aspects of EW at nanoscale.

3.3.1 Contact Angle in EW at Nanoscale

Contact angle is the most well accepted quantity to characterize the wettability of a surface via Young's equation in wetting or L-Y equation in EW. Typically, in EW, an electric field reduces the contact angle. For a macroscopic experimental setup, a droplet is usually deposited on a dielectric, i.e., EWOD. For pure water, the ion concentration is approximately 10^{-7} m, leading to a double layer of thickness ~ 10^{-6} m at the capacitor-liquid interface, restricting the field to an interfacial layer of thickness of Debye length (~10^{-6} m) between the droplet and the dielectric. And the contact angle is determined by the L-Y equation, in which $-\varepsilon\varepsilon_0 |\boldsymbol{E}|^2 D/2$ is the additional electric energy, here D is the thickness of interfacial layer. However, the L-Y equation is no longer valid at nanoscale because the water nanodroplets with size less than the Debye length essentially behave as insulators and the electric field permeates the whole droplet. For nanoscale EW, the disjoining pressure should be considered. So the average electric energy between a nanodroplet and an external electric field is $w_{\mathrm{E}} \sim \sum_i \left\{-|\boldsymbol{E}|\times|\boldsymbol{\mu}_{\mathrm{i}}| L\left[|\boldsymbol{E}|\times|\boldsymbol{\mu}_{\mathrm{i}}|/(k_{\mathrm{B}}T)\right]\right\}$, the physical meaning of the quantities has been explained under equation (6). This suggests that the electric energy depends only on the magnitude of the electric field vector, which is consistent with that at macroscopic scale. Comparing with the L-Y equation, the equation determining the contact angle in EW at nanoscale should be

$$\cos\theta = \cos\theta_0 + \sum_i \frac{|\boldsymbol{E}|\times|\boldsymbol{\mu}_{\mathrm{i}}| L\left[|\boldsymbol{E}|\times|\boldsymbol{\mu}_{\mathrm{i}}|/(k_{\mathrm{B}}T)\right]}{\gamma_{\mathrm{LV}}} \to \cos\theta_0 + \sum_i \frac{|\boldsymbol{E}|^2\times|\boldsymbol{\mu}_{\mathrm{i}}|^2}{3k_{\mathrm{B}}T\gamma_{\mathrm{LV}}}, \quad (31)$$

where θ_0 is the contact angle without electric field.

In addition to the difference in the expressions for the contact angle between EW at macroscopic scale and nanoscale, Daub and coworkers [50, 95] found that the apparent contact angle in EW at nanoscale changes not only as a function of the magnitude of the electric field vector, but also as a function of its direction. In EW, polarization is strongest at liquid surfaces [51]. So the dipolar molecules could be attracted to the liquid-vapor and the solid-liquid interfaces, reducing the interfacial energy. And this could explain the reduction of the contact angle in EW according to the L-Y equation. This explanation suggests that the influence of the electric field on the surface molecules plays an important role in EW. The alignment of the surface molecules in the electric field with different magnitudes and directions could result in different changes of the interfacial tension, which further affects the contact angle. The fraction of surface molecules varies approximately as $1/r_{\mathrm{B}}$, here r_{B} is the base radius of the droplet. For a nanodroplet with r_{B}~3 nm, about 1 out of every 6 or 7 molecules stays in the first surface layer [50], while the fraction is much smaller for a macroscopic droplet. This is why the contact angle in EW at macroscopic scale is insensitive to the direction of the electric field vector.

DOI: 10.7569/RAA.2013.097304

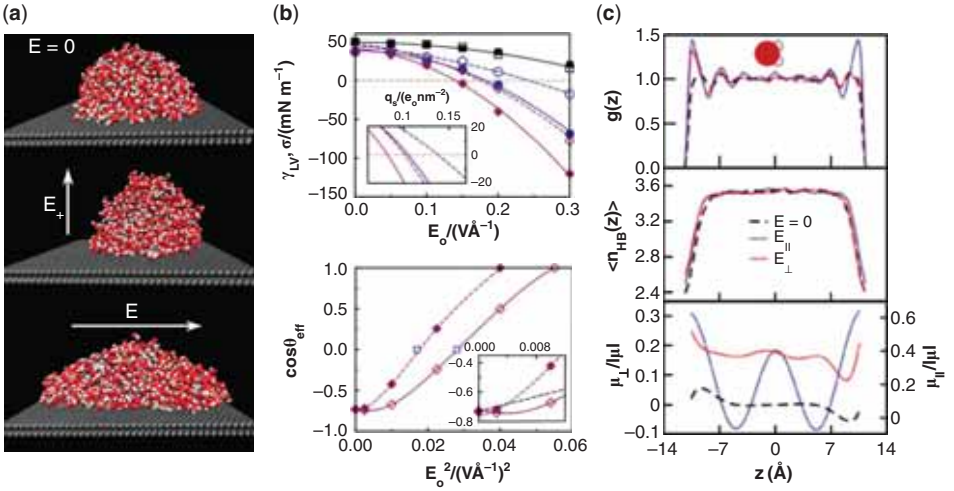

Figure 12 (a) Snapshots of a water droplet with 2000 molecules on a graphite substrate [50]. (b) Upper picture: surface tension γ_{lv} of water with respect to the strength of electric field E_0, applied in the perpendicular (empty) or parallel direction (solid symbols) relative to the surfaces. Lower picture: Hypothetical contact angle $\cos\theta_{eff} = -\sigma/\gamma_{lv}$, illustrating wetting energetics in a parallel (solid) or perpendicular (empty symbols) electric field in a hydrocarbon-like confinement [95]. (c) Density profile $g(z)$, average number of hydrogen bonds per molecules of water $<n_{HB}>$ and orientational polarization of aqueous molecules $\mu_{\perp}$ in a hydrocarbon-like confinement, as a function of the distance from the pore midplane z [95].

Daub and coworkers [50] simulated three cases of EW on graphite at nanoscale by adding the electric energy term $w_E = \sum_i q_i \boldsymbol{r}_i \boldsymbol{E}_0$ to the total potential energy, where the sum was carried over partial charges [113] on oxygen and hydrogen atoms of all water molecules (SPC/E water model). The three cases shown in Figure 12a were EW under the negative electric field perpendicular to the substrate ($\mathbf{E}_-$), positive electric field perpendicular to the substrate ($\mathbf{E}_+$), and the electric field parallel to the substrate **E**. They found that the contact angle was lowered from the field-free result (96.3 ± 1.8°) in all cases studied. For the perpendicular electric field, E_+ produced a reproducibly lower contact angle (84.2 ± 3.9°) than the negative field (89.9±1.5°). In the parallel electric field, the contact angle was asymmetric around the edge of the droplet with the contact angle being 76.3 ± 4.5° at the "leading edge" and 93.6 ± 1.5° or 107.6 ± 5.5° at the "trailing" edge. In another work, they calculated the variation of surface tension with respect to the magnitude and direction of the electric field as shown in Figure 12b [95]. With the increase of the magnitude of the electric field, surface tension decreases, leading to a decrease of the contact angle. When the magnitude of the electric field is the same, surface tension in a parallel electric field is smaller than that in a perpendicular electric

DOI: 10.7569/RAA.2013.097304

field (Figure 12b), consistent with the simulations above. From the simulations, they concluded that, in contrast with measurements in macroscopic systems and predictions from conventional, continuum analyses, there is a notable influence of field direction relative to the interfaces on the contact angle at nanoscale. They attributed this effect to the influence of the electric field on interfacial hydrogen bonding in the water nanodropet.

The orientational bias of surface molecules due to hydrogen bonding couples with the dipoles' response to the electric field. And this coupling determines the dependence of the contact angle on the direction of the electric field. In general, the average number of hydrogen bonds $<n_{HB}>$ is enhanced in the presence of the electric field in agreement with predictions from the theoretical analysis [114]. And the enhancement is larger in a parallel field than in a perpendicular field as shown in Figure 12c. Reduction in $<n_{HB}>$ of about one H bond translates to surface tension contribution of ~ 45 ± 5 mN/m predicted by Luzar *et al.* [115]. So the increase of $<n_{HB}>$ would strongly decrease the interfacial tension and more strongly in parallel field. This is the mechanism of the electric field direction dependent effect of the contact angle in EW at nanoscale.

Another MD study suggested that strong field-induced orientational forces would act on the apolar surface of nanoparticle through water mediation due to the molecular anisotropy of polar solvent molecules [116]. Because of the molecular-level effects, the torque imposed on the nanoparticle (larger than k_BT) exceeds continuum-electrostatics–based estimates by about a factor of 2 and the time scale for reorientation of the nanoparticle decreases dramatically as the field magnitude is increased [117]. A recent research showed that the polarity (sign of the electric field) dependence, observed in EW in neat water, is suppressed in the presence of salt [97]. These findings [118] could provide valuable guidance for electric control of wetting properties at nanoscale, electrically controlled ordering of suspended nanoparticles, the development of chemical sensors or biosensors, and design of NEMS.

3.3.2 Precursor Film in EW

One of the most important problems of the continuum theory developed for wetting or EW is that it will introduce the stress singularity at the three-phase contact line which is similar to the stress singularity at the crack tip. In 1971, Huh and Scriven found that the no-slip boundary condition could induce infinite energy dissipation at the moving contact line, called the Huh-Scriven paradox [119]. De Gennes has pointed out in a famous review in 1985 that "it is only by a patient separation of different physical regimes (Figure 13) that one may hope to reach general laws" [120]. So one of the solutions to the Huh-Scriven paradox is to introduce the micro/nano- new structure in the moving contact line, the precursor film (PF), a molecular layer propagating ahead of the nominal contact line (Figure 13). And it has been realized that the energy dissipation in the precursor film is indeed very strong [121].

DOI: 10.7569/RAA.2013.097304

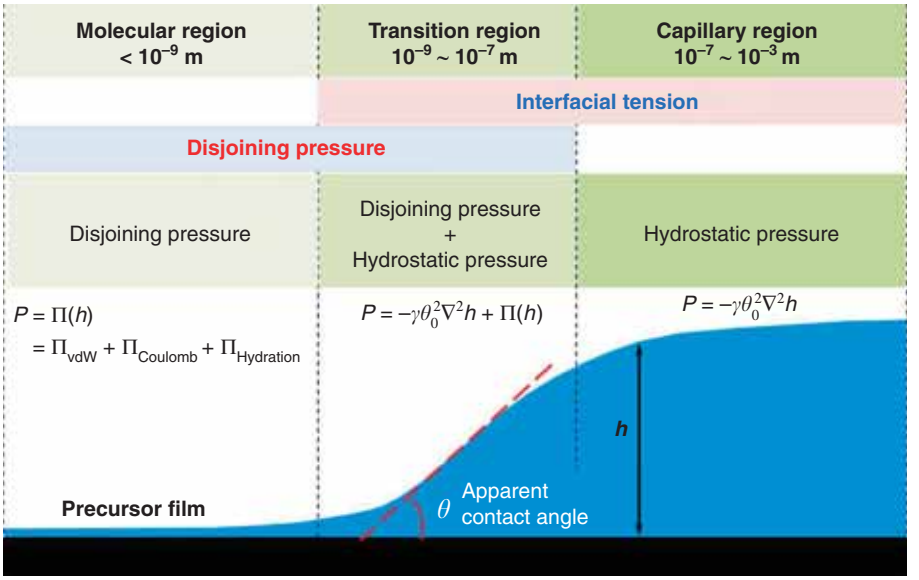

Figure 13 Different physical regimes with different scales in a spreading droplet. In the capillary region, the behavior of the droplet is controlled by the hydrostatic pressure determined by the surface tension of the droplet. In the molecular region, molecular forces, which could be classified into the disjoining pressure, have to be considered to describe the precursor film propagating ahead of the bulk droplet. Between the molecular region and the capillary region is the transition region, where the hydrostatic pressure and the dishoining pressure both dominate.

PF was first proposed by Hardy in 1919 [122]. The existence of the PF has been confirmed by numerous experiments [123–128] and simulations [96, 129]. Through theoretical analysis, de Gennes predicted that the thickness of the PF is on the order of angstrom, while the length of the PF is on the order of micron [120]. So the PF is hard to be detected in experiments for its molecular origin, making the MD simulations of PF necessary.

Recently, Yuan and Zhao have simulated the dynamic spreading of the PF in both wetting and EW on gold surface [52]. In order to imitate the setup of EW, they charged the first layer of the gold substrate and the opposite gold layer. These two gold layers are separated by 10 nm as shown in Figure 14a. The propagation of the PF was found to be fast and even faster in EW following the power law (Figure 14b). Because the polarization is strongest at the interface, the dipolar water molecules could be attracted to the substrate to form the PF in EW. The surface molecules were found to have the strongest mobility (Figure 14c). And the atomic details showed that the fast propagation of the PF is due to continuous and fast diffusion of the surface molecules to the PF. Then the unique properties

DOI: 10.7569/RAA.2013.097304

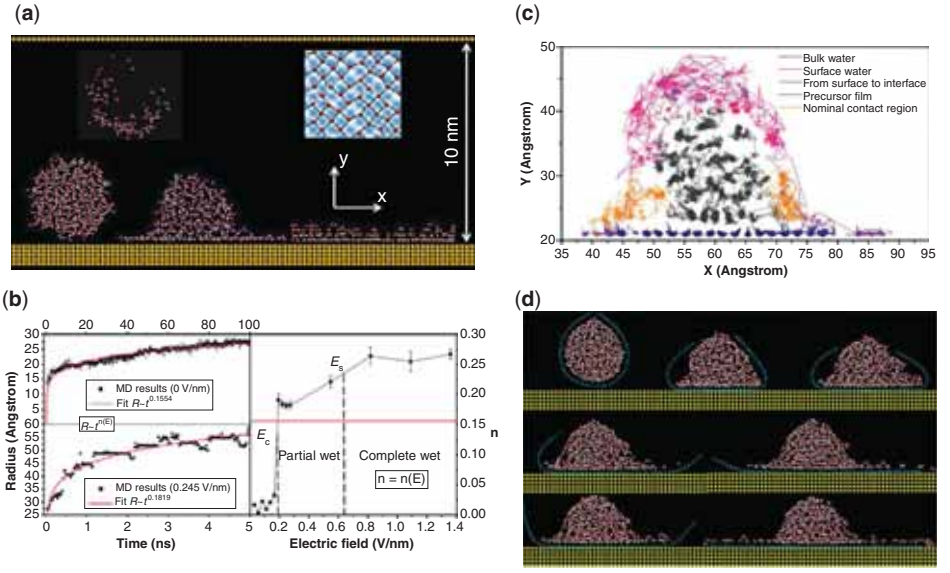

Figure 14 (a) MD simulation domain of wetting and electrowetting. (b) Left: propagation of the radius of the PF with respect to the time. Right: variation of the scaling exponent n with respect to the strength of the electric field. (c) The path lines of water molecules belonging to different regions. (d) The dynamics of EEC obtained by MD simulations [52].

of the PF were studied. It was found that the self-diffusion coefficient D of the PF molecules ($D = 1.132 \times 10^{-5}$ cm^2/s) in wetting is smaller than that of the bulk water ($D = 2.246 \times 10^{-5}$ cm^2/s). In EW, D of the PF decreases to the order of 10^{-6} cm^2/s. So they concluded that the PF is actually no slip and solidlike. And the unique transport properties of the PF are attributed to the 2D hydrogen bonds network found in the PF (Figure 14a).

In addition to the theorectical importance, the PF in EW promises to have a broad range of applications, if the study is extended to the soft and curved substrate. For example, a droplet can be spontanously wrapped by a soft membrane, such as graphene, under certain conditions (Figure 15a). If an electric field is applied to the system, the PF produced would push the folded structure to unwrap the droplet with a force of the order of 10 nN/nm for realizing EEC at nanoscale (Figure 15b and c). Zhu, Yuan and Zhao [96] also found that the competition between two PFs could induce the propagation of capillary wave in EEC (Figure 15c). They reported that the PF driven by the electric field could be drilled into the confined space between the graphene and the substrate. This promises to be a good candidate for delaminating graphene from substrate without damage. Using the unique transport propeties of the PF, EEC can be used for the drug delivery at nanoscale.

DOI: 10.7569/RAA.2013.097304

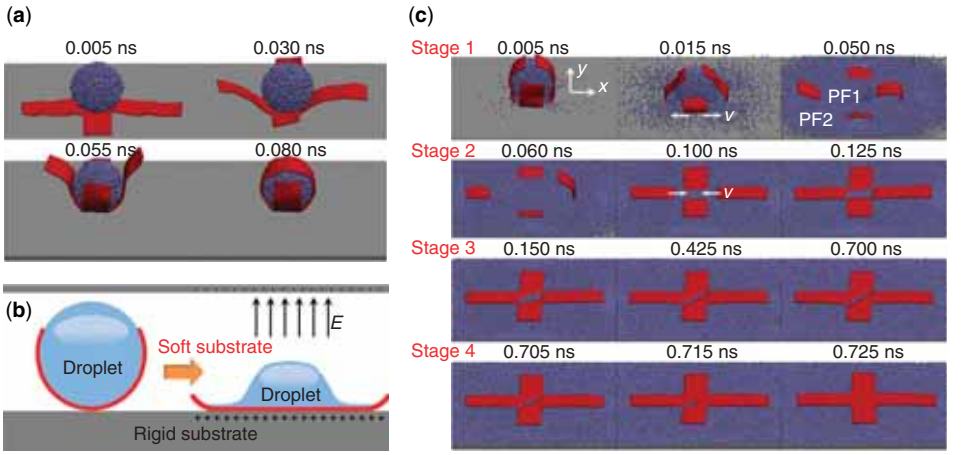

Figure 15 (a) The dynamic EC process of a water droplet wrapped by the graphene. (b) Schematic diagram of EEC at nanoscale, in which the folding structure was pushed by the PF to unwrap the droplet. (c) Capillary wave propagation (borderline between red and ice blue) induced by the competition between PF1 and PF2 during which the graphene was delaminated from the substrate by PF2. Silver, red and ice blue atoms represent graphite, graphene and water atoms, respectively [96].

3.3.3 Molecular Kinetic Theory (MKT)

To explore the effect of an electric field on the dynamic wetting process from the molecular point of view, MKT should be employed. The basic concept of MKT is based on the theory of absolute reaction rates as applied to transport processes and was first proposed by Eyring [130]. In 1969, Cherry and Holmes [131] gave the statistical theory for the interactions between liquid molecules and solid substrate to explain the observation [132] that the rate of spreading of polymers on solid surfaces was dependent on γ_{LV}/η, where η is the viscosity of the polymer, which laid the foundation for MKT. Then Blake and Haynes [133] developed further the above theory and the framework of MKT was formed.

According to MKT, the behavior of the contact line is determined by the adsorption and desorption of the fluid molecules on the surface sites separated by a distance λ (Figure 16). In equilibrium, the fluid molecules on the surface have the same possibility of jumping to left or right. The jump frequency is expressed by

$$\kappa^+ = \kappa^- = \kappa^0 = \frac{k_B T}{h}\frac{F_+}{F_0}\exp\left(\frac{-\Delta G_m}{k_B T}\right), \tag{32}$$

where k_B is the Boltzmann constant, T the temperature, h the Planck constant, F_+ and F_0 the partition functions for the activated and initial states, without loss

DOI: 10.7569/RAA.2013.097304

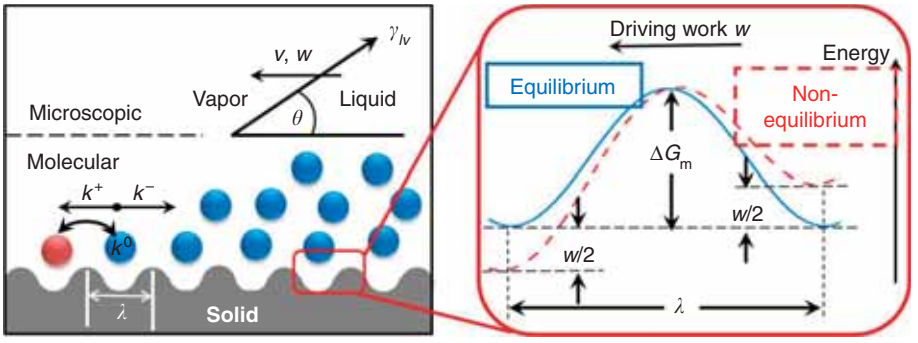

Figure 16 Schematic diagram of the molecular kinetic theory. Left diagram shows fluid molecules jumping on a solid surface with forward jump frequency k^+ and the backward jump frequency k^-. The wavy line above the solid surface represents the potential surface of the interaction between the fluid and the solid. Right diagram is the enlargement of the potential surface with potential well depth ΔG_m, in which the blue line represents the equilibrium state ($k^+ = k^- = k^0$) and the red line non-equilibrium state ($k^+ > k^- \neq k^0$).

of generality one can suppose $F_+ = F_0$, ΔG_m the energy barrier, and k^+ and k^- the frequencies of molecules jumping to the positive and negative directions, respectively. The contact line would move if the adsorption equilibrium is disturbed by the external driving work (the capillary force, van der Waals interactions, electric force, hydration force, etc). The possibility of the fluid molecules jumping to the positive direction is increased and to the negative direction decreased:

$$\begin{cases} \kappa^+ = \dfrac{k_B T}{h}\dfrac{F_+}{F_0}\exp\left(-\dfrac{\Delta G_m}{k_B T}+\dfrac{w}{2nk_B T}\right) \\ \kappa^- = \dfrac{k_B T}{h}\dfrac{F_+}{F_0}\exp\left(-\dfrac{\Delta G_m}{k_B T}-\dfrac{w}{2nk_B T}\right) \end{cases}, \tag{33}$$

where w is the driving work per unit area, n the number of adsorption sites per unit area. So the velocity of the fluid molecules to move forward is

$$v = \lambda\left(\kappa^+ - \kappa^-\right) = 2\kappa^0\lambda\sinh\left(\frac{w}{2nk_B T}\right) = 2\lambda\frac{k_B T}{h}\frac{F_+}{F_0}\exp\left(-\frac{\Delta G_m}{k_B T}\right)\sinh\left(\frac{w}{2nk_B T}\right). \tag{34}$$

From Eq. (34), it is concluded that the motion of the contact line is only controlled by ΔG_m and w. In the above equation, there is a factor $k_B T / h$ having the same dimension as frequency with dimension T^{-1}, called the fundamental frequency, which was first introduced by the Austrian physicist Karl Ferdinand Herzfeld in 1919. And it is an important part in the transition-state theory. At room temperature (T~300 K), $k_B T / h \sim 0.618 \times 10^{13}\ s^{-1}$.

According to Blake's theory [134], the fluid molecules are hindered not only by the interactions with the solid surface (adsorption), but also by the

DOI: 10.7569/RAA.2013.097304

viscous interactions between neighboring fluid molecules. So the energy barrier $\Delta G_{\mathrm{m}}=\Delta G_a+\Delta G_{\mathrm{v}}$, in which ΔG_{a} is the energy dissipation due to the adsorption and ΔG_{v} that due to the viscosity. The relation between the viscosity η of the fluid and ΔG_{v} is $\eta=\left(h/v_{\mathrm{L}}\right)\exp\left(\Delta G_{\mathrm{V}}/k_{\mathrm{B}}T\right)$, where v_{L} is the molecular volume. So the equilibrium jump frequency could be obtained:

$$\kappa^0=\frac{k_{\mathrm{B}}T}{h}\frac{F_+}{F_0}\exp\left(-\frac{\Delta G_{\mathrm{m}}}{k_{\mathrm{B}}T}\right)=\frac{k_{\mathrm{B}}T}{h}\frac{F_+}{F_0}\exp\left(-\frac{\Delta G_{\mathrm{a}}+\Delta G_{\mathrm{v}}}{k_{\mathrm{B}}T}\right)=\frac{k_{\mathrm{B}}T}{\eta v_{\mathrm{L}}}\frac{F_+}{F_0}\exp\left(-\frac{\Delta G_{\mathrm{a}}}{k_{\mathrm{B}}T}\right). \quad (35)$$

Thus, Eq. (34) can be further written as

$$v=2\lambda\frac{k_{\mathrm{B}}T}{\eta v_{\mathrm{L}}}\frac{F_+}{F_0}\exp\left(-\frac{\Delta G_{\mathrm{a}}}{k_{\mathrm{B}}T}\right)\sinh\left(\frac{w}{2nk_{\mathrm{B}}T}\right). \quad (36)$$

In Blake's work, it was supposed that the adsorption contribution ΔG_{a} is equal to the reversible work of adhesion ($Wa=\gamma_{\mathrm{LV}}+\gamma_{\mathrm{SV}}-\gamma_{\mathrm{SL}}$) between the liquid and the solid. In some articles [135, 136], ΔG_{a} was also assumed to be the potential well depth on the solid surface.

To determine the driving work w, different physical regimes should be distinguished. In the capillary region, the capillary force dominates the dynamic wetting behavior (Figure 13). According to Blake's original work, the driving work is

$$w=\gamma_{\mathrm{LV}}\left(\cos\theta^0-\cos\theta\right), \quad (37)$$

where θ^0 is the equilibrium contact angle and θ the dynamic advancing contact angle. In the case of EW, additional term should be added to $\cos\theta^0$. So the driving work [137] is rewritten as

$$w=\gamma_{\mathrm{LV}}\left(\cos\theta_{\mathrm{E}}^0-\cos\theta\right)=\gamma_{\mathrm{LV}}\left[\cos\theta^0+\frac{\varepsilon_0\left(\Phi+\Phi_{\mathrm{m}}\right)^2}{4\gamma_{\mathrm{LV}}\varepsilon_3 K}-\cos\theta\right], \quad (38)$$

in which θ_{E}^0 is the equilibrium contact angle in EW, ε_0 the permittivity of free space, ε_3 the relative permittivity of the surrounding medium, Φ the electric potential, Φ_{m} the electric potential generated by charge on the substrate, K the effective dielectric thickness. Substituting Eq. (38) into Eq. (36), the velocity of the contact line is obtained

$$v=2\lambda\frac{k_{\mathrm{B}}T}{\eta v_{\mathrm{L}}}\frac{F_+}{F_0}\exp\left(-\frac{\Delta G_{\mathrm{a}}}{k_{\mathrm{B}}T}\right)\sinh\left\{\frac{\gamma_{\mathrm{LV}}}{2nk_{\mathrm{B}}T}\left[\cos\theta^0+\frac{\varepsilon_0\left(\Phi+\Phi_{\mathrm{m}}\right)^2}{4\gamma_{\mathrm{LV}}\varepsilon_3 K}-\cos\theta\right]\right\}. \quad (39)$$

In the molecular region, the intermolecular forces should be considered to calculate the diving work. Following Derjaguin and Churaev [138], the movement of a thin film is induced by the gradient of the disjoining pressure $\prod\left(h_{\mathrm{f}}\right)=-dw\left(h_{\mathrm{f}}\right)/dh_{\mathrm{f}}$, which is the variation of the effective interfacial potential with respect to the film thickness h_{f}. In the case of EW, the disjoining pressure is composed of the van

DOI: 10.7569/RAA.2013.097304

der Waals force $\prod_V$, the structural force $\prod_S$ and the electric force $\prod_E$. So the driving work should be

$$w = \int_{h_f}^{\infty} \Pi\left(h_f'\right) h_f' = \int_{h_f}^{\infty} \left[\Pi_V\left(h_f'\right) + \Pi_S\left(h_f'\right) + \Pi_E\left(h_f'\right)\right] dh_f' = w_V + w_S + w_E . \quad (40)$$

Thus, the governing equation for the EW at nanoscale can be written as

$$v = 2\lambda \frac{k_B T}{\eta v_L} \frac{F_+}{F_0} \exp\left(-\frac{\Delta G_a}{k_B T}\right) \sinh\left(\frac{w_V + w_S + w_E}{2nk_B T}\right). \quad (41)$$

The disjoining pressure can also be obtained directly from MD simulations.

Although much progress has been made in the study of EW at nanoscale through MD simulations, there is still plenty of room for developing the MD algorithm considering the interfacial dynamics and electric field. For simulating EW, three issues are of concern. First, it is important to choose the potential for modeling the interactions related to the interface. Currently, Lennard-Jones (LJ) potential is the most widely used model for simulating the interaction between a pair of neutral atoms due to its efficiency. The most common expression for the LJ potential is $V_{ij} = 4\varepsilon_{ij}\left[\left(\sigma_{ij}/r\right)^{12} - \left(\sigma_{ij}/r\right)^{6}\right]$, in which ε_{ij} is the depth of the potential well, σ_{ij} the distance at which the interacting potential is zero, and r the distance between i and j atoms. The repulsive term r^{-12} arises from the Pauli repulsion at short ranges due to overlapping electron orbitals and the attractive term r^{-6} comes from the van der Waals force at long ranges. Because of the fact that the attractive term has its physical origin, the LJ potential is mainly used to model the van der Waals forces in the literature. And many forces fields, whose parameters are based on empirical experimental values or ab inito calculations, have integrated the LJ potential into its energy functional to model the van der Waals interactions. Numerous MD simulations based on LJ potential have obtained reasonable results comparable to the experimental observations. But the LJ potential has its limitations due to the inaccuracy of the repulsive term. To predict the repulsive term more accurately, Buckingham proposed a formula considering the Pauli repulsive energy [10]. But this model also has drawback that the repulsive term converges to a constant, while the attractive term diverges as the interacting distance approximates zero. From the above discussions, we conclude that more accurate interaction potential should be developed to better use MD for EW studies. Second, the potential parameters should be selected carefully to simulate the interactions between dissimilar atoms in the interface. Different combing rules have been proposed to calculate these parameters. But each rule has its scope of applications. Third, how to apply the electric field is vital for simulating EW. There are mainly two methods of imitating the electric field in the literature: adding an electric potential term to the total potential function; and charging the substrate. It should be mentioned that different methods could lead to different results. So it deserves further studies to

DOI: 10.7569/RAA.2013.097304

identity which method can simulate real situation more exactly. And new methods of applying the electric field should also be developed to unearth new phenomena and mechanisms in EW at nanoscale through MD simulations.

4 Experimental Methods and Experiments in EW

Experimental study on EW is becoming an intense research topic all over the world. Most researchers have focused their interests on the fundamental mechanism of EW, controllable transportation of liquid, and novel liquid and substrate materials. In the past few years, there have been many research papers about experimental research on EW (Table 2).

4.1 Fundamental Mechanism of EW

Contact angle saturation has been a key research topic in EW. Basic EW theory predicts that the contact angle will drop to 0 with continually increased voltage. However, in practice, the effect of contact angle saturation has always been observed to limit the contact angle modulation. The physical origin of this phenomenon is still not clear. In 2012, Chevalliot *et al.* conducted a research concerning the EW contact angle saturation [139]. They experimentally demonstrated that when using DC voltage, EW contact angle saturation is invariant with electric field, contact line profile, interfacial tension, choice of non-polar insulating fluid, and type of polar conductive fluid or ionic content. Although this work does not unequivocally prove what causes contact angle saturation, it reveals what factors play a very limited or no role, and how dominant factors causing saturation may change with duration of voltage application.

Just like the mechanism of saturation, contact angle hysteresis is another topic of dispute. Dynamic contact angles and hysteresis under EWOD were investigated by Nelson *et al.* [140]. Measurements were obtained over a wide range of applied EWOD voltages or EW numbers ($0 \le Ew \le 0.9$), and droplet sliding speeds or capillary numbers ($1.4\times10^{-5} \le Ca \le 6.9\times10^{-3}$). Chang and Pak reported the effect of contact angle hysteresis on EW threshold voltage for droplet transport [141]. They reported that the threshold voltage equals the hysteresis voltages in both single-plate and twin-plate configurations and the square root of 2 times the hysteresis voltage in the two-plate configuration by analyzing the contact angles at EW threshold theoretically. They also fabricated devices (Figure 17) using 2.5 μm thick polyimide ($\varepsilon_r = 3.3$) as the dielectric layer and thin Teflon AF as the hydrophobic layer ($\theta_0 = 116°$ and $\alpha = 4–6°$). The experiments showed the threshold voltages for droplet transport initiation of 28, 40, 28 V in the single-plate, two-plate and twin-plate devices, respectively. The experiments also showed the threshold voltages for stable droplet transport of 35, 50 and 35 V, respectively. All the results are in very good agreement with theoretical values.

Droplet under electric field usually has a complex inner fluid field, which includes coupled influence of electric field, thermal field and fluid field. Wang and

DOI: 10.7569/RAA.2013.097304

Table 2 Some recent experimental investigations on EW.

Authors	Droplet Liquids	Substrates	Methods
Chevalliot *et al.* (2012) [139]	Aqueous solution with surfactant	Glass-ITO -Parylene C/HT -Fluoropel 1601V	EW saturation in various situations
Nelson *et al.* (2012) [140]	Water	Cr/Au-SiN-Teflon	Dynamic contact angles and hysteresis under EWOD
Chang and Pak (2012) [141]	Methylene blue	Glass-ITO electrode-polyimide-Teflon AF	Contact angle hysteresis in EW
Ruiter *et al.* (2012) [142]	Aqueous drops with surfactant	Teflon AF	Measurement of dynamic interfacial tensions
Wu and Suzuki (2012) [143]	Hexadecane	Glass-electrode-CYTOP	L-DEPOE
Wang *et al.* (2011) [145]	Water in silicone oil double emulsion droplet	Parallel-plate structure	EWOD & DEP
Wang and Jones (2011) [146]	Oil droplets in water medium		Low voltage DEP
Keng *et al.* (2012) [189]	[^{18}F]FTAG	EWOD electrodes	Purify [^{18}F]FDG by EWOD
Murade *et al.* (2011) [171]	Water droplet in oil	EWOD electrode arrays	Optical switch based on EWOD
Chung *et al.* (2012) [148]	Bubbles	Glass-Au/Cr-PR-Teflon	EW actuation of Bubble
Hu *et al.* (2012) [149]	Water	Carbon Nanotubes	Water-ice transition
Zhang *et al.* (2012) [150]	5 CB liquid crystal	Au-Inhomogeneous Polyimide	Molecular orientation of LC droplet under AC voltage
Hu *et al.* (2012) [151]	6 kinds of ionic liquids	ITO-Parylene C-Teflon	AC EW between 2 plates
Wang *et al.* (2007) [153]	Water	Carbon Nanotube Membrane	Polarity-dependent EW
Wu *et al.* (2012) [157]	Water	ITO-Micro/Nano-structured ZnO layers	Wetting transition
Papadopoulou *et al.* (2012) [159]	Water	Structured metal oxide	EW on nanostructured surface

DOI: 10.7569/RAA.2013.097304

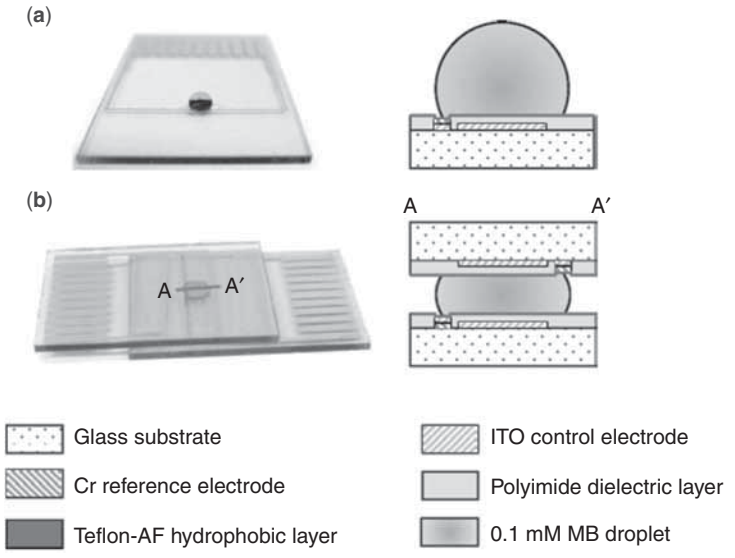

Figure 17 Fabricated electrowetting devices and their cross-sectional schematics. (a) EWOD device in single-plate configuration; (b) EWOD device in twin-plate configuration [141].

Zhao have *in situ* observed the thermal Marangoni convection on the surface of a sessile droplet by infrared thermal imaging and Micro Particle Image Velocimetry (μ-PIV) [47]. In their experiments, droplets are heated by two sources: point heat sources at the top of the droplets (Figure 18a) and planar heat sources on the substrate (Figure 18b). The temperature gradient on the surface of droplet will lead to a surface tension gradient, which will finally result in a severe inner convection, i.e., Marangoni convection. The flow rate inside the droplet is measured to be about 10 mm/s.

EWOD is also used to measure the surface tension of a liquid. Ruiter *et al.* investigated how EWOD could be used to monitor the dynamic liquid-liquid interfacial tension (IFT) with a time resolution of O(1 s) using amplitude modulation of the AC voltage [142]. This method was demonstrated for aqueous drops containing Triton X-100 surfactant on a Teflon AF-coated substrate and with heptane as the immiscible oil ambient.

4.2 Controllable Transportation of a Tiny Droplet

EW is a practical method to manipulate a tiny droplet, consequently, the transportation of a droplet has drawn much interest. Dielectrophoresis is another method for controllable liquid transportation. Many investigations have been carried out to analyze the differences and connection between these two methods. Wu and Suzuki demonstrated such a relationship [143]. They proposed the concept of

DOI: 10.7569/RAA.2013.097304

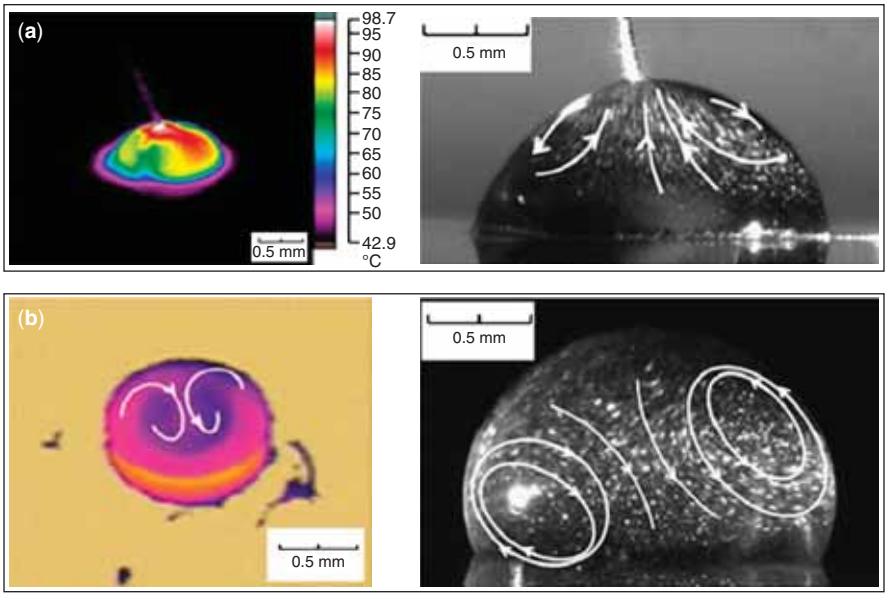

Figure 18 Surface and inner convection of a droplet. (a) Droplet heated by a point heat source; (b) droplet heated by hotplate [47].

"electropolarization" as the origin of driving force for dielectric particles (DEPs), conductive (EWOD) or dielectric liquid (L-DEP). EWOD is regarded to share the same origin, i.e., molecular electropolarization, since the presence of electropolarization force F_p (Figure 19a) near the triple contact layer (TCL), and the resultant stress tension will be involved to balance surface tensions (Figure 19a). By assuming the presence of the nm-order electrical double layer (EDL), they have recovered the L-Y equation and have explained the CA saturation of EWOD.

Wu *et al*. also proposed a novel low-voltage droplet manipulation method using liquid dielectrophoresis on electrets (L-DEPOE), which dramatically reduce the driving voltage to only 5 V for reversely moving the oil droplets [144]. As shown in Figure 19b, by employing an electret, a quasi-permanently charged material which can generate over 1000 V on its surface, a droplet was moved reversely to minimize the system potential energy when a COMS relay switched the potential distribution on the left and right bottom electrodes.

Many valuable investigations have also been carried out in specific areas. Wang *et al*. studied on-chip electric field actuated microfluidic assembly of double emulsion (DE) droplets used for fabrication of cryogenic foam targets [145]. The voltage controllable EWOD and DEP effects make it possible to manipulate both conductive and dielectric droplets simultaneously on a microfluidic chip. They demonstrated that aqueous and nonaqueous liquid droplets can be dispensed

DOI: 10.7569/RAA.2013.097304

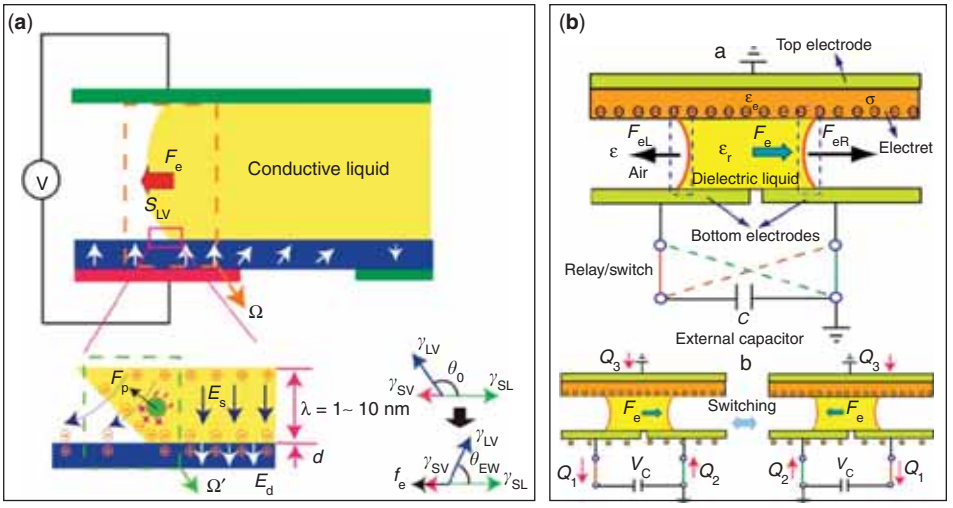

Figure 19 EWOD and L-DEPOE (a) In EWOD conductive liquid molecules far away from solid surfaces are subjected to a zero electric field. Zoom-view of the EDL near the energized electrode. Molecules of conductive liquid are polarized in the non-uniform field near the TCL [143]. (b) L-DEPOE: an external capacitor C is changed over between two bottom electrodes to change electric potential distribution generated by electret, hence the dielectric liquid is driven by L-DEP force to the grounded bottom electrode. L-DEPOE system exchange charges with ground through the two bottom electrodes [144].

from on-chip reservoirs by EWOD and DEP actuations, respectively (Figure 20). Dispensed droplet volume reproducibility was tested over a range of operational parameters, including applied voltage, and length of cutting electrode. By optimizing the operating conditions, they obtained a reproducibility of ±3.0%, which was adequate for the laser target fabrication based on the sensitivity analysis. After dispensing water and oil droplets, these droplets were combined to form DE droplets. They developed the Gibbs free energy model to test the likelihood of DE formation and presented experimental results showing the formation of both water-in-oil and oil-in-water DE droplets in parallel-plate structure.

The follow-up research introduced a new method of actuating oil droplets in water medium that exploited negative DEP to reduce oil actuation voltages. Theoretical modeling and experimental demonstrations for this scheme were presented. The actuation forces on liquid droplets were calculated with an electromechanical model using lumped parameter electromechanics. This model predicted that dielectric droplet actuation can be made compatible with EW-based water droplet manipulation if the oil droplet is immersed in water. Microfluidic operations of transporting, splitting, merging, and dispensing of oil droplets were achieved at a voltage level of ~100 V [146].

DOI: 10.7569/RAA.2013.097304

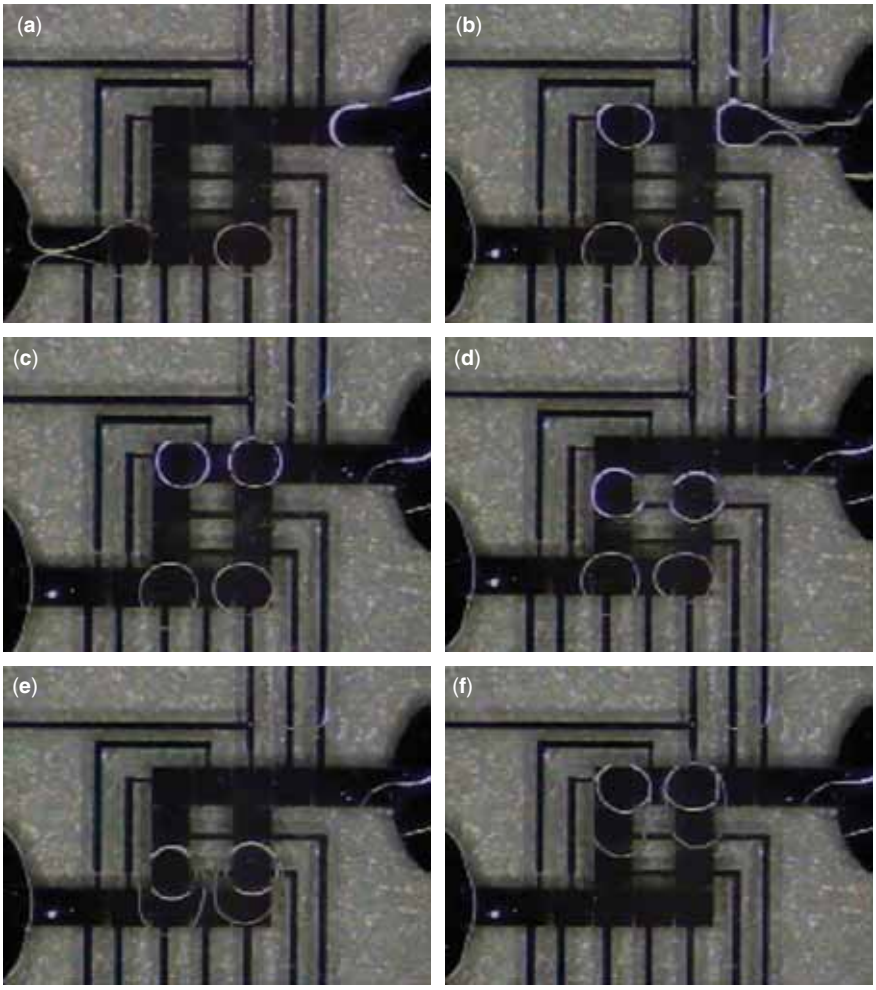

Figure 20 The formation of water-in-silicone oil double emulsion droplets. (a) Two silicone oil droplets are dispensed through DEP actuation by applying 330 Vrms 100 Hz AC voltage; (b) two DI water droplets are dispensed by EWOD actuation by applying 85 Vrms 100 Hz AC voltage; (c), (d) and (e) the water droplets are delivered and combined with oil droplets to form DE droplets; (f) the water droplets pull the wholy merged water-in-oil DE droplets by EWOD actuation [145].

As mentioned earlier, thermocapillary convection, also known as Marangoni convection, has a large influence on the behavior of droplet. Gao *et al*. investigated into a digital liquid transporting chip which could manipulate droplets precisely based on Marangoni force [147]. They found that threshold force for mobilization is a function of droplet size and liquid parameters, and droplet velocity after

DOI: 10.7569/RAA.2013.097304

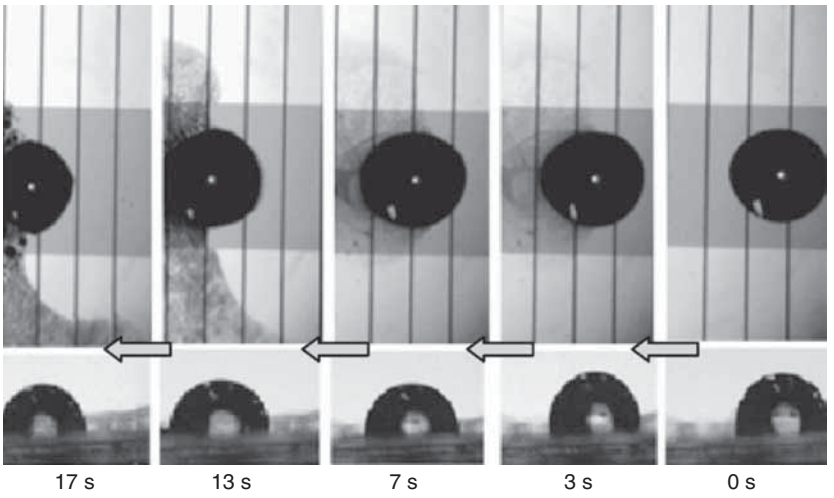

Figure 21 The frame sequence of droplet transportation on a chip. When applied voltage is 7 V, the transportation velocity is about 0.1 mm/s. The top figures show the topview of the movement of the droplet and the figures at the bottom are the sideview of the droplet [147].

depinning is a function of applied thermal gradient, droplet size and liquid parameters. Test results showed that transportation velocity of 3 µl DI water and silicone oil could reach 0.1 mm/s and 1 mm/s, respectively, at a voltage of 7 V (Figure 21). Their finding provides practical guidelines for the design of microfluidic chips based on thermocapillary actuation.

The studies have not only focused on transportation of water and oil droplets, as Chung *et al*. offered a method to manipulate bubbles and other objects with EW [148]. They use AC-EW to oscillate an air bubble in a water medium in order to capture or repel neighboring micro/mini-objects. Experiments showed capturing of various objects including glass beads and fish eggs. They also demonstrated that oscillating bubbles generated a repelling force when the density of neighboring objects was much lower than that of the medium. AC-EW not only oscillates a bubble, but also laterally transports the oscillating bubble on a 2-D surface. Consequently, capture, carrying and release were achieved on a chip without any acoustic excitations for bubble oscillation. They believe that this method may provide an efficient tool for handling micro/mini-objects including biological cells.

EW at nanoscale is also an important research area, especially on CNTs or graphene. Hu *et al*. studied the effect of confinement on water to ice transition temperature [149]. The channels are formed between single-walled carbon nanotubes (SWCNTs) when SWCNT films were treated with diamond wire drawing dies. They dipped a part of SWCNT rope into water, and the electrical property of the SWCNT rope was monitored with decreasing temperature. A sharp jump in voltage was found when the temperature was 274.1 K, which represents the transition

DOI: 10.7569/RAA.2013.097304

temperature of confined water in the channels between SWCNTs. Their results indicated that the temperature of water-ice transition increased due to its confinement in nanoscale channels.

4.3 Various Liquid Samples

Water is not the only liquid which shows EW effect. With the development of liquid crystals (LCs) and ionic liquids, new liquid samples are introduced to EW phenomenon. Zhang *et al*. [150] investigated the oscillation response of dielectric LC droplets during an ac EW on inhomogeneous substrates induced by a pre-rubbed polyimide layer. The EW oscillation amplitude varies ~40% depending on the LC molecular orientation on the substrate. The unique properties of the ac-EW of liquid crystals were revealed in view of the EW driving force, the intermolecular resistance, and the inhomogeneous molecular orientation in LC droplet. The findings provide a potential mechanism to optimize the driving approach for ac-EW of LC droplets by tailoring the substrate.

Ionic liquids are also important in EW research. Hu *et al*. investigated the electrocapillarity of ionic liquids [151]. It shows attractive features involving wide operating temperature and in particular high stability, fast response and good reversibility at high temperatures. Besides, electrocapillarity of ionic liquids is strongly dependent on power supply frequency. Paneru *et al*. studied the behavior when two series of ionic liquids electrowetted a Teflon AF1600 surface [152]. When voltage is applied, the static contact angle decreases from about 150° to 50° (DC voltage) and to 15° (AC voltage). They found excellent reversibility and contact angle hysteresis was minimal (≈2°). They also found that the spreading of the ionic liquid (under DC voltage) was about twice as fast as its retraction (when voltage was switched off). The characteristic time is related to the viscosity of the ionic liquid.

4.4 Wetting Property of New Substrate Materials

There has been considerable interest in substrate materials. Wang and coworkers studied the effect of the application of external potential on wetting control [153, 154]. At a critical bias (~1.7 V), with the membrane acting as anode, there is an abrupt transition from the superhydrophobic to hydrophilic state. This phenomenon is strongly polarity dependent; for a negative bias applied to the membrane, 2 orders of magnitude higher bias is required for the transition. They found that electrochemical oxidation of the nanotube anode was responsible for the observed abrupt transition occurred when the carbon nanotube membrane acted as anode.

They also investigated electrically-controlled wetting and dewetting on rough surfaces comprised of silicon micropillars coated with a hydrophobic material [155]. EW experiments indicated that water droplets wetted the micro-array when the applied voltage was raised beyond a threshold value. When the applied bias is removed, the water droplets can be made to partially dewet the surface and revert

DOI: 10.7569/RAA.2013.097304

back into a stable hydrophobic state by appropriate design of the porosity of the micro-array, the aspect ratio of the micro-pillars and the wetting property of the coating material.

In EW, dielectric layer usually plays the role of bearing a high voltage and being hydrophobic. Papageorgiou *et al*. demonstrated that local delamination of the top coating under high electric fields could be the reason [156]. Thus, improvement in the adhesion strength of the hydrophobic top coating to the main dielectric has been attempted through a plasma-deposited fluorocarbon interlayer. They found the proposed dielectric stack exhibited (a) resistance to dielectric breakdown, (b) higher contact angle modulation range, and (c) EW cycle reversibility.

Other substrates are applied for EW devices. Xia and coworkers studied wetting transition on micro- and nano-structured ZnO layers [157]. Wetting property of hexagonal mesoporous silica was studied by Lu *et al*. [158] Papadopoulou *et al*. also conducted research on EW on silicon and metal oxide [159].

4.5. EW and Coffeering Effect

When a droplet of coffee dries, one usually sees a ring-like pattern left on the substrate, this is called coffee ring, or "coffee stain" effect. As the coffee stain is caused in a particle-laden liquid, researchers have been looking for a way to inhibit it. According to Eral *et al*., EW plays a very important role in coffee stain effect [160]. Mugele's group [160] found that EW significantly inhibited the formation of coffee stain (Figure 22a). In their experiments, one droplet of conducting liquid was placed upon the substrate. The substrate was made up by glass-ITO conductive layer-SU8 (a widely used photoresist) dielectric layer. Polystyrene particles were dispersed in the droplet and the EW was applied by a Pt wire electrode. As the voltage increases, the SU-8 surface tends to be hydrophilic and the contact angle decreases. In the experiments (Figure 22b), ring-like patterns were formed without electric field. However, when AC voltage was applied, the pattern was changed. If the frequency is much lower than the resonance frequency of droplet (< 10 Hz), the contact line of droplet moves. As a consequence, the particles cannot be deposited near the contact line and the contact line is not pinned on the surface. So a smaller fluorescent pattern was found after the evaporation. If the frequency is close to the resonance frequency (~100 Hz to ~ 10 kHz), the triple point moves fast and intense inner flow is formed. So after evaporation, one small spot was found on the surface and no coffee stain was formed. If the frequency reaches 100 kHz or even higher, no significant inner flow is caused. Meanwhile, because of the AC current with high frequency, the droplet is heated. The flow caused by heating depressed the inner flow. So the particles were spread uniformly on the surface and only one fluorescent area was formed. They concluded that AC voltage near the resonance frequency will depress the coffee stain effect.

Kumar, Chuang and Wereley also reported the influence of EW on coffee stain effect [162]. They fabricated a multi-layer substrate to carry out Optical EW (OEW)

DOI: 10.7569/RAA.2013.097304

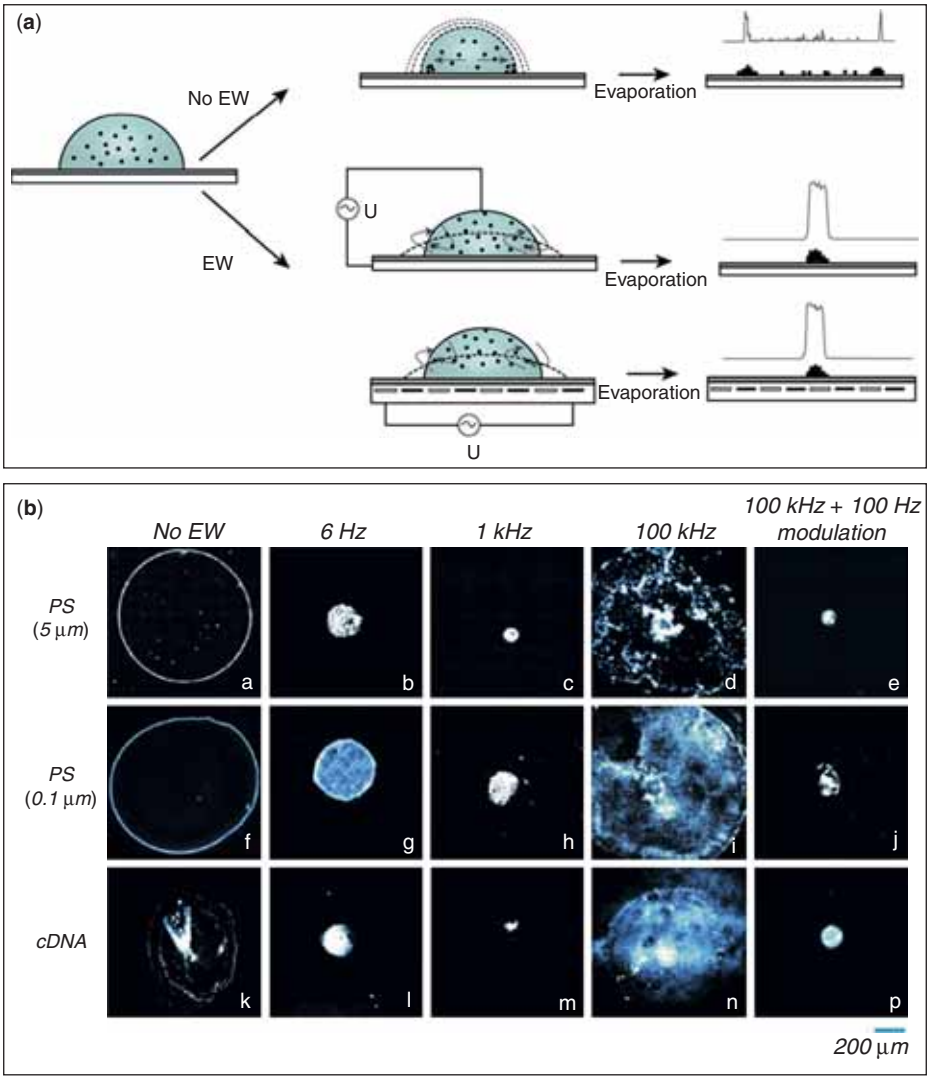

Figure 22 The influence of EW on coffee stain effect. (a) Coffee stain is formed on the substrate only when there is no applied voltage. In the case of electrowetting, coffee stain disappears regardless of the configuration of EW. (b) Experimental results of coffee stain with different types of particles (5 μm, 0.1 μm PS particles and cDNA particles) under different applied voltages (No voltage, 6 Hz, 1 kHz, 100 kHz and 100 kHz + 100Hz modulated AC voltage) [160].

DOI: 10.7569/RAA.2013.097304

experiments. The substrate was composed by glass, ITO, photoconductor, dielectric layer and Teflon hydrophobic layer. They applied 632.8 nm He-Ne laser to guide the droplet to move. At the same time, 1064 nm infrared laser was focused on the bottom side of the substrate. The infrared laser was focused inside the droplet. Because the ITO layer will absorb infrared light and generate heat, they considered the infrared laser spot as a point heat source. Because of this heat source, a thermal convection was formed inside the droplet so the particles will accumulate at this point. As the droplet dries, the coffee stain effect is depressed and a fluorescent spot will appear at the infrared laser spot. If the IR laser is removed, coffee stain pattern can be seen near the triple point.

4.6 EW in a Single-Walled Carbon Nanotube (SWCNT)

In a water-filled single-walled carbon nanotube (SWCNT), because of the thinnest solid part of the interface, quite novel and interesting phenomena have been found. Zhao *et al*. [161] designed a unique device and used a modified "four electrodes" technique to study the coupling between the carriers in SWCNT and the water molecules inside the SWCNT. The devices consist of an individual, suspended SWCNT and 6 electrodes and are fabricated with electron beam lithography patterning (Raith 150, Raith Co.) and Focused Ion Beam (model: FEI Strata DB235). Interesting results were found as shown in Figure 23a.

These results indicate that electrical signals (current/voltage) can switch on/off the flow of water inside the SWCNT. The velocity of flow shows a linear relation with the magnitude of current and its direction depends on that of the current as well as the SWNT carriers' property (electrons or holes). Meanwhile, the flowing water can generate a voltage along the nanotube. The magnitude of induced voltage is closely related to the velocity and the quantity of flowing water inside SWCNT. These observations suggest that the SWCNTs can be exploited as unique, tunable molecular channels for water, which has high potential for application in nanofluidics, drug delivery and nanoscale energy conversion.

It is interesting to note the above discussions have focused on the interface between the SWCNT and water molecules inside the SWCNT. The coupling between SWCNT and molecules outside the SWCNT is also demonstrated to harvest surface energy of polar liquid. Liu *et al*. [163] showed a simple, effective design of SWCNTs to harvest surface energy of ethanol and converted it into electricity as shown in Figure 23b. In this ethanol burner-like design, an open-circuit voltage (V_{oc}) can be obtained as a result of capillary flow in the channels among SWCNTs driven by surface tension and the V_{oc} remains constant as long as there is ethanol present. Meanwhile, the performance (rate of inducing V_{oc} and power output) can be significantly enhanced by Marangoni effect [164]. The maximum power can be up to ~1770 pW per device and can serve as a self-power system to drive thermistors as shown in Figure 23c.

DOI: 10.7569/RAA.2013.097304

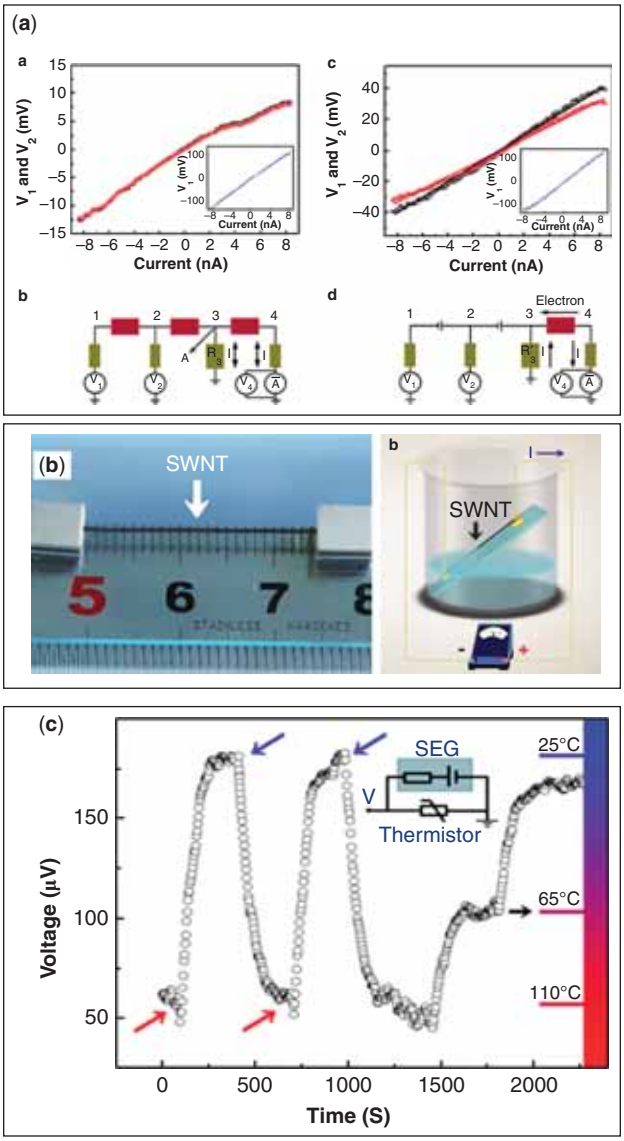

Figure 23 Electric generator based on carbon nanotubes. (a) In vacuum, V_1 (black) and V_2 (red) are almost the same and show linear behavior with applied current between electrodes 3 and 4. However, in water vapor (600 μl), significant difference between V_1 and V_2 can be observed [161]. (b) When measuring, the device is placed into a beaker with an angle between the SWNT rope and ethanol level. (c) Dynamic characteristics of the open-circuit voltage (V_{oc}) are monitored when ethanol is added into the beaker. The voltage drop across the thermistor is detected when the temperature is varying [163].

DOI: 10.7569/RAA.2013.097304

5 Recent Applications of EW

EW, since its emergence, has been not only a scientific phenomenon, but is also a practical technology. Over the last 10 years, EW has already shown its strong competitiveness in the fields of displays [165], liquid lenses [56, 166], micro total analysis systems (μ-TAS) [167], etc.

5.1 EW in Display Technology

Nowadays, display devices based on rugged flexible substrates have become a new growth area of technology, because of their advantages of low cost, easy processing, lightweight, mechanical flexibility, etc. This technology could cause explosive growth of e-reader devices. You and Steckl have demonstrated EW devices fabricated on flexible substrates [168], including paper, polymers (plastics) and metals. Prototypes of flexible EW arrays on plastic substrates are demonstrated to switch reversibly by applying a low voltage difference (20V). These display devices can operate under mechanical bending (Figure 24). These results indicate the promise of flexible EW systems for mobile and other devices.

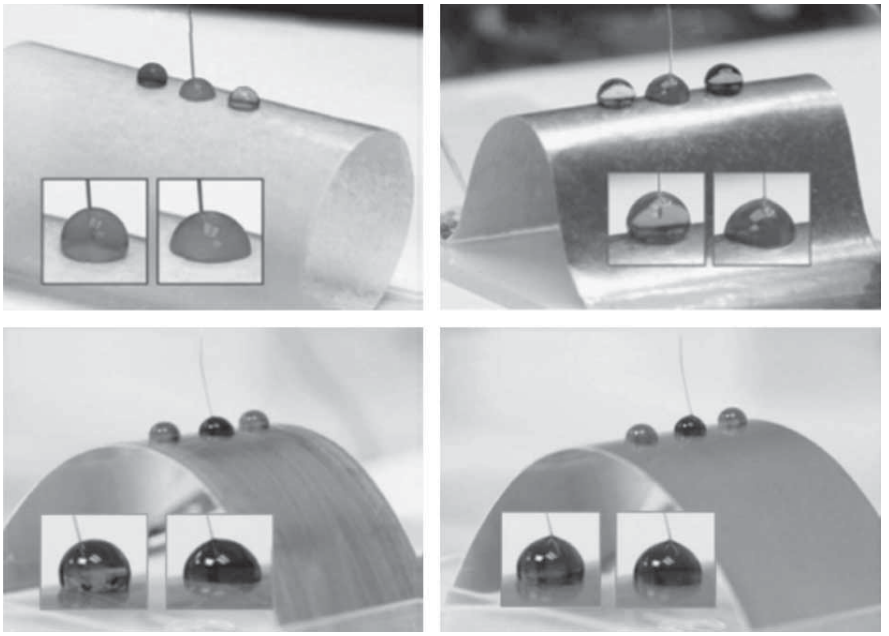

Figure 24 Photographs of electrowetting on various flexible substrates. Different shapes of flexible substrates are used in the experiments. With applied voltage, the contact angles of droplets are apparently shifted [168].

DOI: 10.7569/RAA.2013.097304

5.2 EW in Liquid Lenses

Variable-focus lenses have broad applications in cameras, consumer electronics, and medical instruments. Kang and Yue have reported a novel configuration of variable-focus liquid lens based on EWOD [169]. Their lens consists of a glass slide coated with a conductive ITO film and a hydrophobic dielectric film, a hollow conical metal ring suspended right above the gap between the slide and the ring, and the lens liquid (water). They reported that the new fluid lens works under a relatively low voltage (40 V) and its focus can shift from 2.5 cm to infinity (Figure 25).

Polymers are also possible materials for fluid lenses. Im *et al*. have invented a polymer microlens based on EW [170]. They have fabricated a PDMS microlens array (Figure 26). They fabricated the lenses utilizing an embedded metal (Cr/Au) electrode and parylene/Teflon dielectric layers. The rough surface is in the Cassie-Baxter state with water contact angle (CA)~137°. When the voltage reaches 250 V, the contact angle decreases 63°. The upside-down hanging of the droplet on the substrate is also used to compute the adhesion force of the rough surface.

Figure 25 Images showing the ability of the EW based fluid lens. The focal plane is moved due to the EW effect. The letters 'IM' are placed closer to the lens than the doll. When the applied voltage is changed, the focal plane is moved from near to far, so the letters 'IM' and the doll are sequentially focalized [169].

DOI: 10.7569/RAA.2013.097304

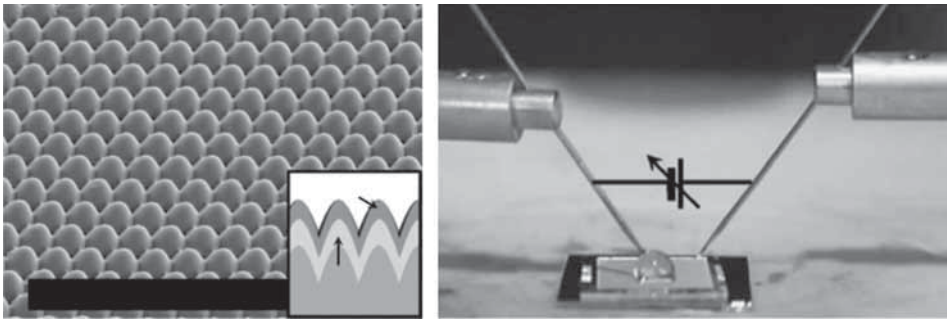

Figure 26 The SEM micrograph of polymer microlens array is shown. The lenses are fabricated with an embedded metal (Cr/Au) electrode and parylene/Teflon dielectric layers. With applied voltage, the contact angle decreases to 63° (V = 250 V) [170].

5.3 EW in Optical Communication

EW is also applied in the field of optical communication. Murade *et al*. demonstrated an EW based optical switch with tunable aperture [171]. Under the influence of an electric field a non-transparent oil film can be replaced locally by a transparent water drop creating an aperture through which light can pass. They demonstrated an array of switchable apertures that can be tuned individually or simultaneously.

5.4 Application of EW in Micro Total Analysis Systems (μ-TAS)

The most focused and most discussed application of EW is in biomedicine. Zhou *et al*. utilized nanostructured ZnO based superhydrophobic high dielectric constant surface to fabricate digital microfluidic device [172]. They studied two fabrication methods for nannosturctured ZnO superhydrophobic surface. Firstly, they used electrochemical deposition methods to fabricate a nanostructured ZnO film, whose dielectric constant is 6.21 and the maximum contact angle is 158.9°. Secondly, they utilized hydrothermal synthesis of ZnO nanorods to achieve a high dielectric constant barrier, in order to prevent electrical leakage. The contact angle of this barrier reaches 164.8° and the contact angle hysteresis is 11.3°. They believed that such superhydrophobic high dielectric constant composite material could increase the performance of μ-TAS.

In the field of medical diagnostic, Zhu *et al*. reported an ELISA chip based on EWOD [173]. Their ELISA chip integrated droplet generation and manipulation functions. They first tested the droplet transportability using silicon test chips with control electrodes, in order to optimize the droplet manipulation. Then, they tested it on ITO chips, which were finally used for an ELISA chip. On the ELISA chip, they carried out immunoassay with rat immunoglobulin G (IgG) and goat anti-rat

DOI: 10.7569/RAA.2013.097304

IgG marked with horseradish peroxidase as an example. The driving velocity of droplets is 5–7 mm/s on the ELISA chip, and a chip-scaled immunoassay can be finished within 20 min by using colorimetric detection, with the volume of the sample and reagents of only 0.5–1 μl.

Tian *et al*. also applied the EWOD technology in biomedicine experiments. They built a micro polymerase chain reaction (μPCR) chip utilizing EWOD to control the temperature uniformity in the microchamber [174]. They mentioned that the sample leakage and evaporation are two major drawbacks in the stationary μPCR system. Experimental results indicated that the system covered with PDMS membrane may hold the methylene blue (MB) solution inside the chamber intact for at least 500 s at 26°C, whereas the remaining aqueous solution is only 30% at 91.2°C. They used EW method in a stationary μPCR chip to lower the contact angle of sidewall, and then filled the reaction chamber completely with the solution. In such cases, evaporation of liquid could be depressed.

5.5 Cell-based Digital Microfluidics: Application of EWOD on Cells

The principal application emerging from EW in controlling droplet position is termed as digital microfluidics (DMF) [175]. In DMF, a droplet containing samples or reagents can be dispensed from reservoirs, moved, merged, and split into smaller droplets by applying a series of electrical potentials to an array of electrodes [176]. DMF has been introduced as a promising platform for cell-based assays, because of automated manipulation of multiple reagents as well as less reagent and analysis time are required. Despite these advantages, cell-based assays on EWOD platform have been difficult due to "biofouling"—biomolecular adsorption of cells and proteins on hydrophobic EWOD surfaces. In order to avoid or reduce it, silicone oil is widely used. The effect of silicone oil is to maintain a film between the droplet and the solid surface [12]. Often a protein called bovine serum albumin (BSA) at very low concentration is added to biological reagents to reduce adhesion of enzymes and proteins to the solid surfaces [177]. Furthermore, specific surfactants like Pluronics have been studied and found to be biocompatible. In a more detailed study, the authors suggested that Pluronic species which have long PPO chain could have a stronger effect in reducing fouling [178]. These advances and others have made DMF compatible with a wide range of applications in chemical biology, including cell-based assays. Two types of cell-assays are described blow:

1. To isolate and concentrate cells on-chip (mainly regarding cell operations)

   The ability to manipulate specific cells individually and isolate them is attractive for cellular biology, though there may be many mechanisms for manipulating cells. Fan *et al.* [179] used dielectrophoresis to separate neuroblastoma cells to different regions of droplets that were manipulated by DMF. The original droplets were then split into daughter droplets containing different cell densities, see Figure 27a. This technique may be useful for on-chip cell

DOI: 10.7569/RAA.2013.097304

concentration for a wide range of applications. Shah *et al.* integrated two technologies: droplet microfluidics using EWOD and individual particle manipulation using optoelectronic tweezers (OETs) [180] or antibody-conjugated magnetic beads (MB-Abs) [181] in one microfluidic device as an automated platform for cellular isolation and analysis.

2. To analyze cell behavior (mainly regarding cell functions analysis)

   Digital microfluidics can also be used to analyze the biological cells and droplet—the carrier. Barbulovic-Nad *et al.* [182] performed a toxicity assay of the surfactant Tween-20, which is lethal to cells. The droplets containing Jurkat-T cells merged with droplets carrying different concentrations of Tween-20 and then mingled again with droplets with cell viability dyes, see Figure 27b. The DMF assay was more sensitive and the actuation by DMF did no harm to cell vitality, which was consistent with Zhou *et al.*'s results [183]. Then Barbulovic-Nad *et al.* [184] developed the first lab-on-a-chip platform for complete adherent cell culture, which is capable of implementing all of the steps—cell seeding, growth, detachment, and re-seeding—on a fresh surface, see Figure 27c. On this basis, cell-based apoptosis [185] and primary

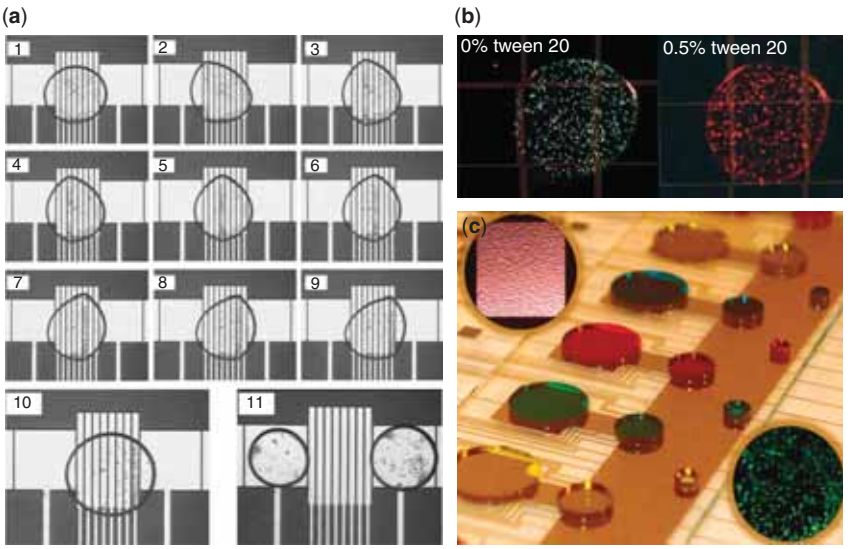

Figure 27 (a) Mammalian cell droplets concentrated by DEP and EWOD. (1) Cells are evenly suspended in a PBS and sucrose solution initially. (2)-(10) Cells are driven by negative DEP and concentrated on the right side of the droplet. (11) Droplet is split by EWOD [179]. (b) cell-based toxicology assays on DMF device. The Jurkat-T cells in the droplet at the left frame with no Tween-20 are alive and fluoresce green when labeled with calcein; in contrast, when exposed to high concentration of Tween-20 they die and fluoresce red when labeled with ethidium homodimer-1 [182]. (c) Photo of a digital microfluidic platform developed for complete cell culture. The inset pictures are the cells in bright field and fluorescence field respectively [184].

DOI: 10.7569/RAA.2013.097304

cell culture [186] assays were implemented by Wheeler's group. Another possible approach to integrate EWOD droplet actuation with adherent cell-based assays is the fabrication of small functional zones in the Teflon-AF matrix where biomolecules [187, 188] are immobilized.

Keng *et al*. have developed an all-electronic digital microfluidic device for microscale chemical synthesis in organic solvents, operated by EW [189]. They demonstrated the multistep synthesis of [^{18}F]FDG, the most common radiotracer for positron emission tomography (PET), with high and reliable radio-fluorination efficiency of [^{18}F]FTAG and quantitative hydrolysis to [^{18}F]FDG. They also showed that batches of purified [^{18}F]FDG could successfully be used for PET imaging in mice and that they passed typical quality control requirement for human use.

6 Unresolved Issues and Prospects

Despite the exciting growth of studies on EW or EWOD in recent years, there are still tremendous opportunities for both research and applications. Many important issues are not clearly understood. Let us mention a few unresolved problems that are of general interest:

1. The dynamic details of EW, especially at micro- and nano-scales, are still unclear; simulation methods for EW such as the phase-field model are still in their initial stages and rely too much on the parameters. Miniaturization and portability are the trend for future applications, so more studies need to be carried out on micro- and nano-EW with flexible substrates.
2. Because of increasing demand from display industry, EW behavior of tiny droplets, at the scale of pico (10^{-12}) liter or even smaller, is becoming a hot research area. For this purpose, new research ideas are also urgently needed, such as EW under Atomic Force Microscope (AFM), Scanning Electron Microscope (SEM), Tunneling Electron Microscope (TEM), etc. Since EW is a multi-field topic, the study of fluid convection inside the droplet is very important. Marangoni convection shows great influence on μPCR chips. Besides, low driving voltage and small contact angle hysteresis are desirable in real applications, so more attention should be paid to developing suitable materials with high quality.
3. For MD simulations on EW or EWOD, the most important issue is that more accurate potentials for modeling interfacial dynamics should be developed to obtain more reasonable results. For EW simulation, how to apply the electric field is also an important issue and deserves to be explored. The applications of the new phenomena, such as the electric field direction-dependent effect on the contact angle in EW at nanoscale, should be further explored. The PF driven by the electric field promises to be a good candidate for actuating the micro/nano structures due to its unique transport properties and

DOI: 10.7569/RAA.2013.097304

deserves detailed investigations. Until now, there has been no report on simulating EW through the reactive force field (ReaxFF) [190]. The ReaxFF was developed for simulating chemical reactions, and it eschews explicit bonds in favor of bond orders, which allows for continuous bond formation/breaking. As a matter of fact, the PF produced during EW could form bonds and hydrogen bond networks on the substrate. Under the electric field, it is also possible to create conditions for chemical reactions, which cannot be observed in MD simulations based on the traditional force field. Thus, it is necessary to use the ReaxFF to simulate EW for validation and verification with other force fields. In addition, the ReaxFF has the advantage that it is more accurate than the traditional MD simulations and more computationally efficient compared with the *ab initio* calculations.

There are, of course, many other important problems. Generally speaking, EW is a combination of multiscale and multi-physical-field problem which should be treated by multiscale methods (Figure 28). Studies combining multiscale theoretical, experimental and simulation aspects will promote EW to more applications.

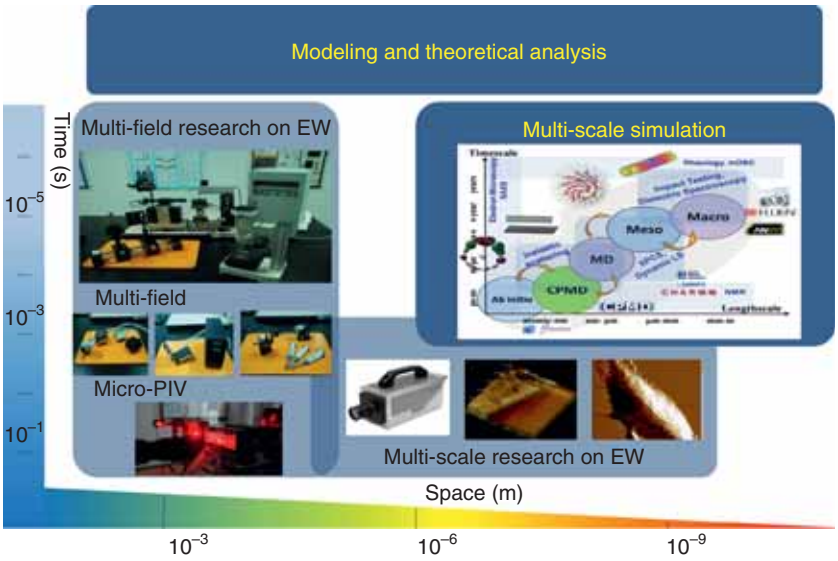

Figure 28 Multifield and multiscale research methods on EW. Experimentally, EW effect on different sizes of droplet (from micrometer to macroscale) can be investigated. With the help of AFM, this can be extended to nanometer scale. In the time scale, high speed CCD can exhibit the movement of droplet in one microsecond. Multi-scale simulation can provide more detailed information for the experiments and it can help to discover new phenomena which are beyond the experimental capability.

DOI: 10.7569/RAA.2013.097304

7 Summary

This article has reviewed the recent research progress on electrowetting (EW) and electrowetting-on-dielectric (EWOD), and has focused mainly on experimental and simulation methods and their main applications. A brief look at the development history of EW was given first, from electrocapillary to EW and then to EWOD. Considering that real surfaces are always rough with topography patterns, extended EW equations were put forward and relevant experiments were conducted. With decreasing system size, EW phenomenon will be different at nanoscopic scale due to large surface-to-volume ratio. Compared to classical EW configuration, variations such as spontaneous EW are being studied. As a good candidate for the drug delivery on micro- and nanoscales, the concept of EEC was introduced. Since flexible substrates with curved surfaces are the trend from an applied perspective, so research on EW with curved surfaces was presented. Then in sections 3 and 4 we discussed experimental and simulation methods in relevant EW experiments and simulations in detail. In the end, some modern applications based on EW technique were presented.

Acknowledgements

This work was jointly supported by the the Key Research Program and the Instrument Developing Project of the Chinese Academy of Sciences (Grant Nos. KJZD-EW-M01 and Y2010031), and National Natural Science Foundation of China (NSFC, Grant Nos. 60936001 and 11072244). The first author also thanks other group memebers (Xueyan Zhu, Ziqian Wang and Jianjun Li) for their support in preparing this review.

Symbols list

B: bending stiffness of hair (N·m)
c: capacitance per unit area (F/m^2)
c: velocity tensor
c_i: component of velocity tensor (m/s)
d: thickness of the dielectric film (μm)
d_h: separation distance between hairs (mm)
D: self-diffusion coefficient (cm^2/s)
E: electric field intensity (V/m)
Ew: EW number (dimensionless number)
E_W^* : curvature-modified EW number
f_i^{eq}: equilibrium distribution function
$\mathbf{F}_e$: electric force (N)
$\mathbf{F}_{st}$: surface tension function (N)
$\mathbf{F}_P$: ponderomotive force (N)

DOI: 10.7569/RAA.2013.097304

$G_{kk'}(\mathbf{x}, \mathbf{x}')$: Green function
ΔG_m : barrier energy (J)
h: Planck's constant (J·s)
$\boldsymbol{J}_\phi$: diffusion flux (m/s)
K: effective dielectric thickness (m)
k_B: Boltzmann's constant (J/K)
L_{dry}: length of the bent part of hair (mm)
L_{EC}: elastocapillary length (mm)
n: number of adsorption sites per unit area (m^{-2})
$\boldsymbol{n}$: unit normal vector
p: pressure (Pa)
R_S: radius of the substrate (m)
S: solid-liquid interface
S_p: spreading parameter (N/m)
Δt: time step (s)
T: absolute temperature (K)
$\mathbf{u}$: velocity vector (m/s)
v: velocity (m/s)
V: voltage (V).
$W(\phi)$: a bistable potential
w: driving work per unit area (J/m^2)
z: a phenomenological parameter
a: d/R_S, ratio of the dielectric film thickness to the substrate radius
β : viscosity coefficient parameter
γ_{LV}: liquid-vapor surface tension (N/m)
γ_{SL}: solid-liquid interfacial tension (N/m)
γ_{SV}: solid-vapor interfacial tension (N/m)
δ: a small positive parameter
ε: dielectric constant (F/m)
ζ: a parameter far less than 1
η: viscosity ($kg \cdot m^{-1} \cdot s^{-1}$)
θ: contact angle (°)
k: frequency (s^{-1})
λ: separation distance of surface sites (nm)
$\boldsymbol{\mu}_i$: electric dipole moment (C·m)
$\prod$: disjoining pressure (N/m^2)
ρ: mass density (kg/m^3)
r_0: constant free parameter (kg/m^3)
σ: amount of charge (C)
σ_e: surface charge density (C/m^2)
τ: relaxation parameter
$\boldsymbol{\tau}$: unit tangent vector
τ_L: line tension (N)

DOI: 10.7569/RAA.2013.097304

Φ: electrical potential (V)
χ: geodesic curvature at the contact point (m^{-1})
ϕ : phase-field parameter
Ω: domain occupied by the two phases (liquid and vapor)

References

1. L. Minnema, H. A. Barneveld and P. D. Rinkel, An investigation into the mechanism of water treeing in polyethylene high-voltage cables. *IEEE Trans. Electrical Insulation* **15**, 461–472 (1980).
2. G. Beni and S. Hackwood, Electro-wetting displays. *Appl. Phys. Lett* **38**, 207–209 (1981).
3. G. Lippmann, Relation entre les phenomenes electriques et capillaries. *Ann. Chim. Phys.* **5**, 494–549 (1875).
4. B. Berge, Electrocapillarity and wetting of insulator films by water. Comptes Rendus Acad. Sci. II 317, 157–163 (1993).
5. C. Quilliet and B. Berge, Electrowetting: A recent outbreak. *Curr. Opin. Colloid Interface Sci.* **6**, 34–39 (2001).
6. M. G. Pollack, A. D. Shenderov and R. B. Fair, Electrowetting-based actuation of droplets for intergrated microfluidics. *Lab Chip* **2**, 96–101 (2002).
7. S. K. Cho, H. Moon and C. J. Kim, Creating, transporting, cutting, and merging liquid droplets by electrowetting-based actuation for digital microfluidic circuits. *J. Microelectromech. Syst.* **12**, 70–80 (2003).
8. S. Kuiper and B. H. W. Hendriks, Variable-focus liquid lens for miniature cameras. *Appl. Phys. Lett.* **85**, 1128–1130 (2004).
9. R. A. Hayes and B. J. Feenstra, Video-speed electronic paper based on electrowetting. *Nature* **425**, 383–385 (2003).
10. Y. P. Zhao, *Physical Mechanics of Surfaces and Interfaces (in Chinese)*, Science Press, Beijing (2012).
11. F. Mugele and J. C. Baret, Electrowetting: From basics to applications. *J. Phys. Condens. Matter.* **17**, 705–774 (2005).
12. J. Berthier, *Microdrops and Digital Microfluidics*, William Andrew Publishing, Norwich, NY (2008).
13. K. H. Kang, How electrostatic fields change contact angle in electrowetting. *Langmuir* **18**, 10318–10322 (2002).
14. B. Berge and J. Peseux, Variable focal lens controlled by an external voltage: An application of electrowetting. *Eur. Phys. J. E* **3**, 159–163 (2000).
15. T. Krupenkin, S. Yang and P. Mach, Tunable liquid microlens. *Appl. Phys. Lett* **82**, 316–318 (2003).
16. F. Krogmann, W. Monch and H. Zappe, A MEMS-based variable micro-lens system. *J. Optics A* 8, 330–336 (2006).
17. M. A. Bucaro, P. R. Kolodner, J. A. Taylor, A. Sidorenko, J. Aizenberg and T. N. Krupenkin, Tunable liquid optics: Electrowetting-controlled liquid mirrors based on self-assembled janus tiles. *Langmuir* **25**, 3876–3879 (2009).
18. N. Chronis, G. L. Liu, K. H. Jeong and L. P. Lee, Tunable liquid-filled microlens array integrated with microfluidic network. *Opt. Express* **11**, 2370–2378 (2003).

DOI: 10.7569/RAA.2013.097304

19. S. K. Fan, H. Yang and W. Hsu, Droplet-on-a-wristband: Chip-to-chip digital microfluidic interfaces between replaceable and flexible electrowetting modules. *Lab Chip* **11**, 343–347 (2011).
20. J. A. Rogers, Z. Bao, K. Baldwin, A. Dodabalapur, B. Crone, V. R. Raju, V. Kuck, H. Katz, K. Amundson, J. Ewing and P. Drzaic, Paper-like electronic displays: Large-area rubber-stamped plastic sheets of electronics and microencapsulated electrophoretic inks. Proc. Natl. Acad. Sci. USA 98, 4835–4840 (2001).
21. H. You and A. J. Steckl, Three-color electrowetting display device for electronic paper. *Appl. Phys. Lett.* **97**, 023514 (2010).
22. J. Heikenfield, P. Drzaic, J. S. Yeo and T. Koch, Review paper: a critical review of the present and future prospects for electronic paper. *J. Soc. Information Display* **19**, 129–156 (2011).
23. V. Srinivasan, V. K. Pamula and R. B. Fair, An integrated digital microfluidic lab-on-a-chip for clinical diagnostics on human physiological fluids. *Lab Chip* **4**, 310–315 (2004).
24. J. Y. Yoon and R. L. Garrel, Preventing biomolecular adsorption in electrowetting-based biofluidic chips. *Anal. Chem.* **75**, 5097–5102 (2003).
25. A. R. Wheeler, H. Moon, C. J. Kim, J. A. Loo and R. L. Garrell, Electrowetting-based microfluidics for analysis of peptides and proteins by matrix-assisted laser desorption/ionization mass spectrometry. *Anal. Chem.* **76**, 4833–4838 (2004).
26. R. B. Fair, A. Khlystov, T. D. Tailor, V. Ivanov, R. D. Evans, P. B. Griffin, S. Vijay, V. K. Pamula, M. G. Pollack and J. Zhou, Chemical and biological applications of digital-microfluidic devices. *IEEE Design & Test of Computers* 24, 10–24 (2007).
27. C. Karuwan, K. Sukthang, A. Wisitsoraat, D. Phokharatkul, V. Pattnanasettakul, W. Wechsatol and A. Tuantranont, Electrochemical detection on electrowetting-on-dielectric digital microfluidic chip. *Talanta* **84**, 1384–1389 (2011).
28. D. M. Ratner, E. R. Murphy, M. Jhunjhunwala, D. A. Snyder, K. F. Jensen and P. H. Seeberger, Microreactor-based reaction optimization in organic chemistry—Glycosylation as a challenge. *Chem. Commun.* **5**, 578–580 (2005).
29. M. Pollack, A. Shenderov and R. Fair, Electrowetting-based actuation of droplets for integrated microfluidics. *Lab Chip* **2**, 96–101 (2002).
30. W. J. J. Welters and L. G. J. Fokkink, Fast electrically switchable capillary effects. *Langmuir* **14**, 1535–1538 (1998).
31. H. Moon, S. K. Cho and R. L. Garrell, Low voltage electrowetting-on-dielectric. *J. Appl. Phys.* **92**, 4080–4087 (2002).
32. M. Vallet, M. Vallade and B. Berge, Limiting phenomena for the spreading of water on polymer films by electrowetting. *Eur. Phys. J. B* **11**, 583–591 (1999).
33. H. J. J. Verheijen and M. W. J. Prins, Reversible electrowetting and trapping of charge model and experiments. *Langmuir* **15**, 6616–6620 (1999).
34. J. Berthier, Ph. Clementz, O. Raccurt, D. Jary, P. Claustre, C. Peponnet and Y. Fouillet, Computer aided design of an EWOD microdevice. *Sensors Actuators A* **127**, 283–294 (2006).
35. A. Quinn, R. Sedev and J. Ralston, Contact angle saturation in electrowetting. *J. Phys. Chem. B* **109**, 6268–6275 (2005).
36. D. Klarman, D. Andelman and M. Urbakh, A model of electrowetting, reversed electrowetting, and contact angle saturation. *Langmuir* **27**, 6031–6043 (2011).
37. A. Papathanasiou and A. Boudouvis, Manifestation of the connection between dielectric breakdown strength and contact angle saturation in electrowetting. *Appl. Phys. Lett* **86**, 164102 (2005).

DOI: 10.7569/RAA.2013.097304

38. W. Dai and Y. P. Zhao, An electrowetting model for rough surfaces under low voltage. *J. Adhesion Sci. Technol.* **22**, 217–229 (2008).
39. V. Bahadur and S. V. Garimella, Electrowetting-based control of static droplet states on rough surfaces. *Langmuir* **23**, 4918–4924 (2007).
40. T. N. Krupenkin, J. A. Taylor, T. M. Schneider and S. Yang, From rolling ball to complete wetting: The dynamic tuning of liquids on nanostructured surfaces. *Langmuir* **20**, 3824–3827 (2004).
41. D. L. Herbertson, C. R. Evans, N. J. Shirtcliffe, G. McHale and M. I. Newton, Electrowetting on superhydrophobic SU-8 patterned surfaces. *Sensors Actuators A* **130**, 189–193 (2006).
42. Y. Wang and Y. P. Zhao, Electrowetting on curved surfaces. *Soft Matter* **8**, 2599–2606 (2012).
43. J. Berthier, P. Dubois, P. Clementz, P. Claustre, C. Peponnet and Y. Fouillet, Actuation potentials and capillary forces in electrowetting based microsystems. *Sensors Actuators A* **134**, 471–479 (2007).
44. M. G. Pollack, R. B. Fair and A. D. Shenderov, Electrowetting-based actuation of liquid droplets for microfluidic applications. *Appl. Phys. Lett* **77**, 1725–1726 (2000).
45. J. T. Feng, F. C. Wang and Y. P. Zhao, Electrowetting on a lotus leaf. *Biomicrofluidics* **3**, 022406 (2009).
46. N. A. Patankar, On the modeling of hydrophobic contact angles on rough surfaces. *Langmuir* **19**, 1249–1253 (2003).
47. Z. Q. Wang and Y. P. Zhao, In situ observation of thermal Marangoni convection on the surface of a sessile droplet by infrared thermal imaging. *J. Adhesion Sci. Techno.l* **26**, 2177–2188 (2012).
48. S. H. Ko, H. Lee and K. H. Kang, Hydrodynamic flows in electrowetting. *Langmuir.* **24**, 1094–1101 (2008).
49. R. Digilov, Charge-induced modification of contact angle: The secondary electrocapillary effect. *Langmuir* **16**, 6719–6723 (2000).
50. C. D. Daub, D. Bratko, K. Leung and A. Luzar, Electrowetting at the nanoscale. *J. Phys. Chem. C* **111**, 505–509 (2007).
51. V. Ballenegger and J. P. Hansen, Dielectric permittivity profiles of confined polar fluids. *J. Chem. Phys.* **122**, 114711 (2005).
52. Q. Z. Yuan and Y. P. Zhao, Precursor film in dynamic wetting, electrowetting, and electro-elasto-capillarity. *Phys. Rev. Lett* **104**, 246101 (2010).
53. L. Y. Yeo and H. C. Chang, Static and spontaneous electrowetting. *Mod. Phys. Lett. B* **19**, 549–570 (2005).
54. L. Y. Yeo and H. C. Chang, Electrowetting films on parallel line electrodes. *Phys. Rev. E* **73**, 011605 (2006).
55. H. C. Chang and L. Y. Yeo, *Electrokinetically Driven Microfluidics and Nanofluidics*, Cambridge University Press, New York (2010).
56. W. C. Nelson and C. J. Kim, Droplet actuation by electrowetting-on-dielectric (EWOD): A review. *J. Adhesion Sci. Technol.* 26, 1747–1771 (2012).
57. Y. S. Yu, Substrate elastic deformation due to vertical component of liquid-vapor interfacial tension. *Appl. Math. Mech.* **33**, 1095–1114 (2012).
58. J. Bico, B. Roman, L. Moulin and A. Boudaoud, Adhesion: Elastocapillary coalescence in wet hair. *Nature* **432**, 690–690 (2004).

DOI: 10.7569/RAA.2013.097304

59. F. Vollrath and D. T. Edmonds, Modulation of the mechanical properties of spider silk by coating with water. *Nature* **340**, 305–307 (1989).
60. S. Jung, P. M. Reis, J. James, C. Clanet and J. W. M. Bush, Capillary origami in nature. *Phys. Fluids* **21**, 091110 (2009).
61. C. Py, P. Reverdy, L. Doppler, J. Bico, B. Roman and C. N. Baroud, Capillary origami: Spontaneous wrapping of a droplet with an elastic sheet. *Phys. Rev. Lett.* **98**, 156103 (2007).
62. X. Y. Guo, H. Li, B. Y. Ahn, E. B. Duoss, K. J. Hsia, J. A. Lewis and R. G. Nuzzo, Two- and three-dimensional folding of thin film single-crystalline silicon for photovoltaic power applications. *Proc. Natl. Acad. Sci. USA* **106**, 20149–20154 (2009).
63. T. Jamin, C. Py and E. Falcon, Instability of the origami of a ferrofluid drop in a magnetic field. *Phys. Rev. Lett.* **107**, 204503 (2011).
64. J. W. van Honschoten, J. W. Berenschot, T. Ondarçuhu, R. G. P. Sanders, J. Sundaram, M. Elwenspoek and N. R. Tas, Elastocapillary fabrication of three-dimensional microstructures. *Appl. Phys. Lett.* **97**, 014103 (2010).
65. N. Patra, B. Y. Wang and P. Kral, Nanodroplet activated and guided folding of graphene nanostructures. *Nano Lett.* **9**, 3766–3771 (2009).
66. A. Antkowiak, B. Audoly, C. Josserand, S. Neukirch and M. Rivetti, Instant fabrication and selection of folded structures using drop impact. *Proc. Natl. Acad. Sci. USA* **108**, 10400 (2011).
67. M. Pineirua, J. Bico and B. Roman, Capillary origami controlled by an electric field. *Soft Matter* **6**, 4491–4496 (2010).
68. Z. Q. Wang, F. C. Wang and Y. P. Zhao, Tap dance of water droplet. *Proc. R. Soc. A* **468**, 2485–2495 (2012).
69. D. Y. Kim and A. J. Steckl, Electrowetting on paper for electronic paper display. *ACS Appl. Mater. Interfaces* **2**, 3318–3323 (2010).
70. M. Abdelgawad, S. L. S. Freire, H. Yang and A. R. Wheeler, All-terrain droplet actuation. *Lab Chip* **8**, 672–677 (2008).
71. J. Y. Chen, A. Kutana, C. P. Collier and K. P. Giapis, Electrowetting in carbon nanotubes. *Science* **310**, 1480–1483 (2005).
72. G. Wolansky and A. Marmur, The actual contact angle on a heterogeneous rough surface in three dimensions. *Langmuir* **14**, 5292–5297 (1998).
73. S. Chen and G. D. Doolen, Lattice Boltzmann method for fluid flows. *Annu. Rev. Fluid Mech* **30**, 329–364 (1998).
74. X. W. Shan and H. D. Chen, Lattice Boltzmann model for simulating flows with multiple phases and components. *Phys. Rev. E* **47**, 1815–1819 (1993).
75. X. W. Shan and G. Doolen, Multicomponent Lattice-Boltzmann model with interparticle interaction. *J. Stat. Phys.* **81**, 379–393 (1995).
76. M. R. Swift, W. R. Osborn and J. M. Yeomans, Lattice Boltzmann simulation of nonideal fluids. *Phys. Rev. Lett* **75**, 830–833 (1995).
77. M. R. Swift, E. Orlandini, W. R. Osborn and J. M. Yeomans, Lattice Boltzmann simulations of liquid-gas and binary fluid systems. *Phys. Rev. E* **54**, 5041–5052 (1996).
78. D. J. Holdych, D. Rovas, J. G. Georgiadis and R. O. Buckius, An improved hydrodynamics formulation for multiphase flow Lattice-Boltzmann models. *Int. J. Mod. Phys. C* **9**, 1393–1404 (1998).
79. H. B. Li and H. P. Fang, Lattice Boltzmann simulation of electrowetting. *Eur. Phys. J. Special Topics* **171**, 129–133 (2009).

DOI: 10.7569/RAA.2013.097304

80. Y. H. Qian, D. Dhumieres and P. Lallemand, Lattice BGK models for Navier-Stokes equation. *Europhys. Lett.* **17**, 479–484 (1992).
81. H. B. Li and H. P. Fang, Hysteresis and saturation of contact angle in electrowetting on a dielectric simulated by the Lattice Boltzmann method. *J. Adhesion Sci. Technol.* **26**, 1873–1881 (2012).
82. L. Clime, D. Brassard and T. Veres, Numerical modeling of the splitting of magnetic droplets by multiphase Lattice Boltzmann equation. *J. Appl. Phys.* **105**, 07B517 (2009).
83. R. Mei, W. Shyy, D. Yu and L. S. Luo, Lattice Boltzmann method for 3-D flows with curved boundary. *J. Comput. Phys.* **161**, 680–699 (2000).
84. L. Clime, D. Brassard and T. Veres, Numerical modeling of electrowetting processes in digital microfluidic devices. *Comput. Fluids* **39**, 1510–1515 (2010).
85. L. Clime, D. Brassard and T. Veres, Numerical modeling of electrowetting transport processes for digital microfluidics. *Microfluid. Nanofluid* **8**, 599–608 (2010).
86. H. Aminfar and M. Mohammadpourfard, Lattice Boltzmann method for electrowetting modeling and simulation. *Comput. Meth. Appl. Mech. Eng.* **198**, 3852–3868 (2009).
87. H. Aminfar and M. Mohammadpourfard, Droplets merging and stabilization by electrowetting: Lattice Boltzmann study. *J. Adhesion Sci. Technol.* **26**, 1853–1871 (2012).
88. J. J. Huang, C. Shu, J. J. Feng and Y. T. Chew, A phase-field-based hybrid Lattice-Boltzmann finite-volume method and its application to simulate droplet motion under electrowetting control. *J. Adhesion Sci. Technol.* **26**, 1825–1851 (2012).
89. D. Bonn, J. Eggers, J. Indekeu, J. Meunier and E. Rolley, Wetting and spreading. *Rev. Mod. Phys.* **81**, 739–805 (2009).
90. M. A. Fontelos, G. Grun, U. Kindelan and F. Klingbeil, Numerical simulation of static and dynamic electrowetting. *J. Adhesion Sci. Technol.* **26**, 1805–1824 (2012).
91. T. D. Blake, The physics of moving wetting lines. *J. Colloid. Interface. Sci* **299**, 1–13 (2006).
92. R. B. Schoch, J. Y. Han and P. Renaud, Transport phenomena in nanofluidics. *Rev. Mod. Phys.* **80**, 839–883 (2008).
93. L. Bocquet and E. Charlaix, Nanofluidics, from bulk to interfaces. *Chem. Soc. Rev.* **39**, 1073–1095 (2010).
94. Y. X. Li, J. L. Xu and D. Q. Li, Molecular dynamics simulation of nanoscale liquid flows. *Microfluid. Nanofluid* **9**, 1011–1031 (2010).
95. D. Bratko, C. D. Daub, K. Leung and A. Luzar, Effect of field direction on electrowetting in a nanopore. *J. Am. Chem. Soc.* **129**, 2504–2510 (2007).
96. X. Y. Zhu, Q. Z. Yuan and Y. P. Zhao, Capillary wave propagation during the delamination of graphene by the precursor films in electro-elasto-capillarity. *Scientific Reports* **2**, 927 (2012).
97. C. D. Daub, D. Bratko and A. Luzar, Electric control of wetting by salty nanodrops: Molecular dynamics simulations. *J. Phys. Chem. C* **115**, 22393–22399 (2011).
98. J. Liu, M. R. Wang, S. Chen and M. O. Robbins, Uncovering molecular mechanisms of electrowetting and saturation with simulations. *Phys. Rev. Lett* **108**, 216101 (2012).
99. T. H. Yen, Investigation of the effects of perpendicular electric field and surface morphology on nanoscale droplet using molecular dynamics simulation. *Mol. Simul* **38**, 509–517 (2012).
100. A. Kutana and K. P. Giapis, Atomistic simulations of electrowetting in carbon nanotubes. *Nano Lett.* **6**, 656–661 (2006).
101. S. Banerjee, S. Murad and I. K. Puri, Preferential ion and water intake using charged carbon nanotubes. *Chem. Phys. Lett.* **434**, 292–296 (2007).

DOI: 10.7569/RAA.2013.097304

102. X. J. Gong, J. Y. Li, H. J. Lu, R. Z. Wan, J. C. Li, J. Hu and H. P. Fang, A charge-driven molecular water pump. *Nature Nanotechnol.* **2**, 709–712 (2007).
103. G. H. Hu, A. J. Xu, Z. Xu and Z. W. Zhou, Dewetting of nanometer thin films under an electric field. *Phys. Fluids* **20**, 102101 (2008).
104. L. Wang, Z. Q. Zhang and H. W. Zhang, Electrowetting in double-walled carbon nanotubes: Molecular dynamics simulations. *Acta. Phys. Sinica.* **57**, 7069–7077 (2008).
105. Y. Xu and N. R. Aluru, Carbon nanotube screening effects on the water-ion channels. *Appl. Phys. Lett.* **93**, 043122 (2008).
106. Y. T. Wang, Disordering and reordering of ionic liquids under an external electric field. *J. Phys. Chem. B* **113**, 11058–11060 (2009).
107. H. W. Zhang, Z. Q. Zhang and L. Wang, Molecular dynamics simulations of electrowetting in double-walled carbon nanotubes. *Curr. Appl. Phys.* **9**, 750–754 (2009).
108. C. L. Wang, B. Zhou, P. Xiu and H. P. Fang, Effect of surface morphology on the ordered water layer at room temperature. *J. Phys. Chem. C* **115**, 3018–3024 (2011).
109. B. X. Xu, Y. Qiao, Q. L. Zhou and X. Chen, Effect of electric field on liquid infiltration into hydrophobic nanopores. *Langmuir* **27**, 6349–6357 (2011).
110. H. F. Ye, H. W. Zhang, Z. Q. Zhang and Y. G. Zheng, Water sheared by charged graphene sheets. *J. Adhesion Sci. Technol.* **26**, 1897–1908 (2012).
111. Y. L. Zhao, K. Dong, X. M. Liu, S. J. Zhang, J. J. Zhu and J. J. Wang, Structure of ionic liquids under external electric field: A molecular dynamics simulation. *Mol. Simul* **38**, 172–178 (2012).
112. B. Mahar, C. Laslau, R. Yip and Y. Sun, Development of carbon nanotube-based sensors—A review. *Sensors J. IEEE* **7**, 266–284 (2007).
113. H. J. C. Berendsen, J. R. Grigera and T. P. Straatsma, The missing term in effective pair potentials. *J. Phys. Chem.* **91**, 6269–6271 (1987).
114. S. J. Suresh, A. V. Satish and A. Choudhary, Influence of electric field on the hydrogen bond network of water. *J. Chem. Phys.* **124**, 074506 (2006).
115. A. Luzar, S. Svetina and B. Zeks, The contribution of hydrogen-bonds to the surface-tension of water. *Chem. Phys. Lett.* **96**, 485–490 (1983).
116. D. Bratko, C. D. Daub and A. Luzar, Water-mediated ordering of nanoparticles in an electric field. *Faraday Discuss* **141**, 55–66 (2009).
117. C. D. Daub, D. Bratko, T. Ali and A. Luzar, Microscopic dynamics of the orientation of a hydrated nanoparticle in an electric field. *Phys. Rev. Lett.* **103**, 207801 (2009).
118. C. D. Daub, D. Bratko and A. Luzar, *Multiscale Molecular Methods in Applied Chemistry*, Springer, Berlin (2012).
119. C. Huh and L. E. Scriven, Hydrodynamic model of steady movement of a solid/liquid/fluid contact line. *J. Colloid Interface Sci.* **35**, 85–101 (1971).
120. P. G. de Gennes, Wetting: Statics and dynamics. *Rev. Mod. Phys.* **57**, 827–863 (1985).
121. H. Hervet and P. G. de Gennes, The dynamics of wetting - Precursor films in the wetting of dry solids. Comptes. Rendus. *Acad. Sci. II* **299**, 499–503 (1984).
122. W. B. Hardy, The spreading of fluids on glass. *Philos. Mag.* **38**, 49–55 (1919).
123. D. Ausserré, A. M. Picard and L. Léger, Existence and role of the precursor film in the spreading of polymer liquids. *Phys. Rev. Lett.* **57**, 2671–2674 (1986).
124. L. Léger, M. Erman, A. M. Guinet-Picard, D. Ausserré and C. Strazielle, Precursor film profiles of spreading liquid drops. *Phys. Rev. Lett.* **60**, 2390–2393 (1988).
125. F. Heslot, N. Fraysse and A. M. Cazabat, Molecular layering in the spreading of wetting liquid drops. *Nature* **338**, 640–642 (1989).

DOI: 10.7569/RAA.2013.097304

126. E. G. Bortchagovsky and L. N. Tarakhan, Precursor film of a spreading drop of liquid crystal. *Phys. Rev. B* **47**, 2431–2434 (1993).
127. H. P. Kavehpour, B. Ovryn and G. H. McKinley, Microscopic and macroscopic structure of the precursor layer in spreading viscous drops. *Phys. Rev. Lett.* **91**, 196104 (2003).
128. H. Xu, D. Shirvanyants, K. Beers, K. Matyjaszewski, M. Rubinstein and S. S. Sheiko, Molecular motion in a spreading precursor film. *Phys. Rev. Lett.* **93**, 206103 (2004).
129. E. B. Webb, G. S. Grest and D. R. Heine, Precursor film controlled wetting of Pb on Cu. *Phys. Rev. Lett.* **91**, 236102 (2003).
130. S. Gladstone, K. Laidler and H. Eyring. *The Theory of Rate Processes*, McGraw-Hill Book Company, New York (1941).
131. B. W. Cherry and C. M. Holmes, Kinetics of wetting of surfaces by polymers. *J. Colloid Interface Sci.* **29**, 174–176 (1969).
132. S. Newman, Kinetics of wetting of surfaces by polymers - Capillary flow. *J. Colloid Interface Sci.* **26**, 209–213 (1968).
133. T. D. Blake and J. M. Haynes, Kinetics of liquid/liquid displacement. *J. Colloid Interface Sci* **30**, 421–423 (1969).
134. T. D. Blake and J. De Coninck, The influence of solid-liquid interactions on dynamic wetting. *Adv. Colloid Interface Sci.* **96**, 21–36 (2002).
135. Q. Z. Yuan and Y. P. Zhao, Topology-dominated dynamic wetting of the precursor chain in a hydrophilic interior corner. *Proc. Roy. Soc. A* **468**, 310–322 (2012).
136. F. C. Wang and Y. P. Zhao, Slip boundary conditions based on molecular kinetic theory: The critical shear stress and the energy dissipation at the liquid–solid interface. *Soft Matter.* **7**, 8628–8634 (2011).
137. T. D. Blake, A. Clarke and E. Stattersfield, An investigation of electrostatic assist in dynamic wetting. *Langmuir* **16**, 2928–2935 (2000).
138. B. V. Derjaguin and N. V. Churaev, Structural component of disjoining pressure. *J. Colloid Interface Sci.* **49**, 249–255 (1974).
139. S. Chevalliot, S. Kuiper and J. Heikenfeld, Experimental validation of the invariance of electrowetting contact angle saturation. *J. Adhesion Sci. Technol* **26**, 1909–1930 (2012).
140. W. C. Nelson, P. Sen and C. J. Kim, Dynamic contact angles and hysteresis under electrowetting-on-dielectric. *Langmuir* **27**, 10319–10326 (2011).
141. J. H. Chang and J. J. Pak, Effect of contact angle hysteresis on electrowetting threshold for droplet transport. *J. Adhesion Sci. Technol.* **26**, 2105–2111 (2012).
142. R. D. Ruiter, P. Wennink, A. G. Banpurkar, M. H. G. Duits and F. Mugele, Use of electrowetting to measure dynamic interfacial tensions of a microdrop. *Lab Chip* **12**, 2832–2836 (2012).
143. T. Wu and Y. Suzuki, Liquid dielectrophoresis on electret : **A** novel approach towards CMOS-driven digital microfluidics. *J. Adhesion Sci. Technol.* **26**, 2025–2045 (2012).
144. T. Wu, Y. Suzuki and N. Kasagi, Low-voltage droplet manipulation using liquid dielectrophoresis on electrets. *J. Micromech. Microeng.* **20**, 085043 (2010).
145. W. Q. Wang, T. B. Jones and D. R. Harding, On-chip double emulsion droplet assembly using electrowetting-on-dielectric and dielectrophoresis. *Fusion Sci. Technol.* **59**, 240–249 (2011).
146. W. Q. Wang and T. B. Jones, Microfluidic actuation of insulating liquid droplets in a parallel-plate device. *J. Phys. Conf. Ser* **301**, 012057 (2011).
147. A. Gao, X. Liu, T. Li, X. L. Gao and Y. L. Wang, Thermocapillary actuation of droplets on a microfluidic chip. *J. Adhesion Sci. Technol.* **26**, 2165–2176 (2012).

DOI: 10.7569/RAA.2013.097304

148. S. K. Chung, J. O. Kwon and S. K. Cho, Manipulation of micro/miniobjects by AC-electrowetting-actuated oscillating bubbles: Capturing, carrying and releasing. *J. Adhesion Sci. Technol.* **26**, 1965–1983 (2012).
149. L. J. Hu, J. Liu, F. Yu, C.Y. Qiu, H. Q. Zhou, H. C. Yang, M. J. Chen and L. F. Sun, Water–ice transition at 274.1 K in the channels between single-walled carbon nanotubes. *J. Adhesion Sci. Technol.* **26**, 2017–2023 (2012).
150. X. J. Zhang, Y. Huang, Y. Y. Wang, Y. Tian and Y. G. Meng, Effects of inhomogeneous substrate and molecular orientation on the AC electrowetting behavior of liquid crystal droplet. *J. Adhesion Sci. Technol.* **26**, 1985–2000 (2012).
151. X. D. Hu, S. G. Zhang, C. Qu, Q. H. Zhang, L. J. Lu, X. Y. Ma, X. P. Zhang and Y. Q. Deng, Electrically switchable capillarity of ionic liquids. *J. Adhesion Sci. Technol.* **26**, 2069–2078 (2012).
152. M. Paneru, C. Priest, J. Ralston and R. Sedev, Electrowetting of ionic liquids on Teflon AF1600 in ambient hexadecane. *J. Adhesion Sci. Technol.* **26**, 2047–2067 (2012).
153. Z. K. Wang, L. J. Ci, L. Chen, S. Nayak, P. M. Ajayan and N. Koratkar, Polarity-dependent electrochemically controlled transport of water through carbon nanotube membranes. *Nano Lett.* **7**, 697–702 (2007).
154. Z. K. Wang, Y. Ou, T. M. Lu and N. Koratkar, Wetting and electrowetting properties of carbon nanotube templated parylene films. *J. Phys. Chem. B* **111**, 4296–4299 (2007).
155. Z. K. Wang and N. Koratkar, Electrically controlled wetting and dewetting transition on silicon micro-pillar arrays. *Adv. Sci. Lett.* **1**, 222–225 (2008).
156. D. P. Papageorgiou, E. P. Koumoulos, C. A. Charitidis, A. G. Boudouvis and A. G. Papathanasiou, Evaluating the robustness of top coatings comprising plasma-deposited fluorocarbons in electrowetting systems. *J. Adhesion Sci. Technol.* **26**, 2001–2015 (2012).
157. J. Wu, J. Xia, J. Chen, W. Lei and B. P. Wang, Wetting transition on micro/nanostructured ZnO layers. *J. Adhesion Sci. Technol.* **26**, 2099–2104 (2012).
158. W. Lu, A. Han, T. Kim, B. J. Chow and Y. Qiao, Endcapping treatment of inner surfaces of a hexagonal mesoporous silica. *J. Adhesion Sci. Technol.* **26**, 2135–2141 (2012).
159. E. L. Papadopoulou, V. Zorba, E. Stratakis and C. Fotakis, Properties of silicon and metal oxide electrowetting systems. *J. Adhesion Sci. Technol.* **26**, 2143–2163 (2012).
160. H. B. Eral, A. D. Mampallil, M. H. G. Duits and F. Mugele, Suppressing the coffee stain effect: How to control colloidal self-assembly in evaporating drops using electrowetting. *Soft Matter.* **7**, 4954–4958 (2011).
161. Y. C. Zhao, L. Song, K. Deng, Z. Liu, Z. X. Zhang, Y. L. Yang, C. Wang, H. F. Yang, A. Z. Jin, Q. Luo, C. Z. Gu, S. S. Xie and L. F. Sun, Individual water-filled single-walled carbon nanotubes as hydroelectric power converters. *Adv. Mater.* **20**, 1772–1775 (2008).
162. A. Kumar, H. S. Chuang and S. T. Wereley, Dynamic manipulation by light and electric fields: Micrometer particles to microliter droplets. *Langmuir* **26**, 7656–7660 (2010).
163. Z. Liu, K. H. Zheng, L. J. Hu, J. Liu, C. Y. Qiu, H. Q. Zhou, H. B. Huang, H. F. Yang, M. Li, C. Z. Gu, S. S. Xie, L. J. Qiao and L. F. Sun, Surface-energy generator of single-walled carbon nanotubes and usage in a self-powered system. *Adv. Mater.* **22**, 999–1003 (2010).
164. L. E. Scriven and C. V. Sternling, The Marangoni effects. *Nature* **187**,186–188 (1960).
165. P. Sureshkumar and S. S. Bhattacharyya, Display applications of electrowetting. *J. Adhesion Sci. Technol.* **26**, 1947–1963 (2012).
166. C. P. Chiu, T. J. Chiang, J. K. Chen, F. C. Chang, F. H. Ko, C. W. Chu, S. W. Kuo and S. K. Fan, Liquid lenses and driving mechanisms: A review. *J. Adhesion Sci. Technol.* **26**, 1773–1788 (2012).

DOI: 10.7569/RAA.2013.097304

167. T. H. Lin and D. J. Yao, Applications of EWOD systems for DNA reaction and analysis. *J. Adhesion Sci. Technol* **26**, 1789–1804 (2012).
168. H. You and A. J. Steckl, Electrowetting on flexible substrates. *J. Adhesion Sci. Technol.* **26**, 1931–1939 (2012).
169. M. Kang and R. F. Yue, Variable-focus liquid lens based on EWOD. *J. Adhesion Sci. Technol.* **26**, 1941–1946 (2012).
170. M. Im, K. Choi, D. H. Kim, J. H. Lee, J. B. Yoon and Y. K. Choi, Adhesion force change by electrowetting on polymer microlens array. *J. Adhesion Sci. Technol.* **26**, 2079–2086 (2012).
171. C. U. Murade, J. M. Oh, D. V. D. Ende and F. Mugele, Electrowetting driven optical switch and tunable aperture. *Opt. Express* **19**, 15525–15531 (2011).
172. J. Zhou, S. Yang, X. Y. Zeng, J. H. Wu, G. P. Chen and Y. P. Huang, Superhydrophobic ZnO for EWOD digital microfluidic device for application in Micro Total Analysis System (μ-TAS). *J. Adhesion Sci. Technol.* **26**, 2087–2098 (2012).
173. L. Zhu, Y. Y. Feng, X. Y. Ye, J. Y. Feng, J. B. Wu and Z. Y. Zhou, An ELISA chip based on an EWOD microfluidic platform. *J. Adhesion Sci. Technol.* **26**, 2113–2124 (2012).
174. H. Tian, J. Qin, T. Deng, R. Zhang, C. Liu, T. H. Wang and Z. W. Liu, Evaporation phenomenon in micro polymerase chain reaction (μPCR) system and a possible electrowetting solution. *J. Adhesion Sci. Technol.* **26**, 2125–2134 (2012).
175. A. R. Wheeler, Putting electrowetting to work. *Science* **322**, 539–540 (2008).
176. M. J. Jebrail and A. R. Wheeler, Let's get digital: Digitizing chemical biology with microfluidics. *Curr. Opin. Chem. Biol* **14**, 574–581 (2010).
177. V. Srinivasan, V. K Pamula, M. G Pollack and R. B. Fair, A digital microfluidic biosensor for multianalyte detection. *Proc. IEEE 16th Annu. Int. Conf. Micro Electro Mech. Syst.* 327–330 (2003).
178. S. H. Au, P. Kumar and A. R. Wheeler, A new angle on Pluronic additives: Advancing droplets and understanding in digital microfluidics. *Langmuir* **27**, 8586–8594 (2011).
179. S. K. Fan, P. W. Huang, T. T. Wang and Y. H. Peng, Cross-scale electric manipulations of cells and droplets by frequency-modulated dielectrophoresis and electrowetting. *Lab Chip* **8**, 1325–1331 (2008).
180. G. J. Shah, A. T. Ohta, E. P. Y. Chiou, M. C. Wu and C. J. Kim, EWOD-driven droplet microfluidic device integrated with optoelectronic tweezers as an automated platform for cellular isolation and analysis. *Lab Chip* **9**, 1732–1739 (2009).
181. G. J. Shah, J. L. Veale, Y. Korin, E. F. Reed, H. A. Gritsch and C. J. Kim. Specific binding and magnetic concentration of CD8+ T-lymphocytes on electrowetting-on-dielectric platform. *Biomicrofluidics* **4**, 044106 (2010).
182. I. Barbulovic-Nad, H. Yang, P. S. Park and A. R. Wheeler, Digital microfluidics for cell-based assays. *Lab Chip* **8**, 519–526 (2008).
183. J. Zhou, L. Lu, K. Byrapogu, D. M. Wootton, P. I. Lelkes and R. Fair, Electrowetting-based multi-microfluidics array printing of high resolution tissue construct with embedded cells and growth factors. *Virtual Phys. Prototyping* **2**, 217–223 (2007).
184. I. Barbulovic-Nad, S. H. Au and A. R. Wheeler, A microfluidic platform for complete mammalian cell culture. *Lab Chip* **10**, 1536–1542 (2010).
185. D. Bogojevic, M. D. Chamberlain, I. Barbulovic-Nad and A. R. Wheeler, A digital microfluidic method for multiplexed cell-based apoptosis assays. *Lab Chip* **12**, 627–634 (2012).

DOI: 10.7569/RAA.2013.097304

186. S. Srigunapalan, I. A. Eydelnant, C. A. Simmons and A. R. Wheeler, A digital microfluidic platform for primary cell culture and analysis. *Lab Chip* **12**, 369–375 (2012).
187. D. Witters, N. Vergauwe, S. Vermeir, F. Ceyssens, S. Liekens, R. Puers and J. Lammertyn, Biofunctionalization of electrowetting-on-dielectric digital microfluidic chips for miniaturized cell-based applications. *Lab Chip* **11**, 2790–2794 (2011).
188. N. Vergauwe, D. Witters, F. Ceyssens, S. Vermeir, B. Verbruggen, R. Puers and J. Lammertyn, A versatile electrowetting-based digital microfluidic platform for quantitative homogeneous and heterogeneous bio-assays. *J. Micromech. Microeng.* **21**, 054026 (2011).
189. P. Y. Keng, S. Chen, H. J. Ding, S. Sadeghi, G. J. Shah, A. Dooraghi, M. E. Phelps, N. Satyamurthy, A. F. Chatziioannou, C. J. Kim and R. M. V. Dam, Micro-chemical synthesis of molecular probes on an electronic microfluidic device. *Proc. Natl. Acad. Sci. USA* **109**, 690–695 (2012).
190. A. C. T. van Duin, S. Dasgupta, F. Lorant and W. A. Goddard, ReaxFF: A reactive force field for hydrocarbons. *J. Phys. Chem. A* 105, 9396–9409 (2001).

DOI: 10.7569/RAA.2013.097304

